

# LEARNING ROBUST DIFFUSION MODELS FROM IMPRECISE SUPERVISION

Dong-Dong Wu<sup>1,2</sup>    Jiacheng Cui<sup>3</sup>    Wei Wang<sup>1,2</sup>  
 Zhiqiang Shen<sup>3</sup>    Masashi Sugiyama<sup>1,2</sup>

<sup>1</sup>The University of Tokyo, Tokyo, Japan    <sup>2</sup>RIKEN AIP, Tokyo, Japan

<sup>3</sup>Mohamed bin Zayed University of Artificial Intelligence, Abu Dhabi, UAE

## ABSTRACT

Conditional diffusion models have achieved remarkable success in various generative tasks recently, but their training typically relies on large-scale datasets that inevitably contain imprecise information in conditional inputs. Such supervision, often stemming from noisy, ambiguous, or incomplete labels, will cause condition mismatch and degrade generation quality. To address this challenge, we propose *DMIS*, a unified framework for training robust Diffusion Models from Imprecise Supervision, which is the first systematic study within diffusion models. Our framework is derived from likelihood maximization and decomposes the objective into generative and classification components: the generative component models imprecise-label distributions, while the classification component leverages a diffusion classifier to infer class-posterior probabilities, with its efficiency further improved by an optimized timestep sampling strategy. Extensive experiments on diverse forms of imprecise supervision, covering tasks of image generation, weakly supervised learning, and noisy dataset condensation demonstrate that *DMIS* consistently produces high-quality and class-discriminative samples.

## 1 INTRODUCTION

Diffusion models (DMs) (Ho et al., 2020; Song et al., 2020; Karras et al., 2022) have emerged as powerful generative frameworks that have unprecedented capabilities in generating realistic data (He et al., 2025; Yang et al., 2024; Ho et al., 2022). With the classifier guidance (Ho & Salimans, 2022; Dhariwal & Nichol, 2021), conditional diffusion models (CDMs) extended the capabilities of DMs by conditioning the generation process on additional information, such as text descriptions or class labels. These models have demonstrated remarkable performance in various tasks, including text-to-image synthesis (Rombach et al., 2022; Saharia et al., 2022), image inpainting (Zhao et al., 2024; Corneanu et al., 2024), and super-resolution (Esser et al., 2024; Xie et al., 2025).

Unfortunately, the conditioning information required by CDMs is often imprecise in real-world scenarios. When sourced from the internet or obtained through crowdsourcing, such information can be affected by factors such as privacy constraints or limited annotator expertise, leading to various imperfections. In particular, the conditioning data may contain noise, exhibit ambiguity, or suffer from missing and incomplete annotations. We refer to such cases collectively as imprecise supervision (Chen et al., 2024a), where the provided conditioning information is not fully aligned with the true underlying labels. This includes scenarios such as noisy-label data (Li et al., 2017; Wei et al., 2021), partial-label data (Wang et al., 2025b;a), and supplementary-unlabeled data (He et al., 2023). These forms of imprecise supervision can introduce incorrect inductive biases during training and severely affect the reliability and generalization of CDMs.

To address this, several recent studies have proposed adaptations of diffusion models to handle imprecise supervision, such as noise-robust diffusion models (Na et al., 2024; Li et al., 2024) and positive-unlabeled diffusion models (Takahashi et al., 2025). However, these approaches often focus on specific types of imprecise supervision. Moreover, many of them rely on strong external priors to guide the learning process. For example, Na et al. (2024) estimated a noise transition matrix using external noisy-label learning methods, and Li et al. (2024) required risk confidence scores associated with noisy samples. These diffusion-based methods not only rely on prior knowledge from data

or previous techniques, but are also designed with task-specific architectures for particular types of supervision. Such reliance and structural complexity limit their applicability and efficiency in practice. There remains a need for a unified framework that can robustly train CDMs under diverse forms of imprecise supervision without requiring strong prior assumptions.

In this paper, to train a robust CDM in a unified manner, we first formulate the overall learning objective as a likelihood maximization problem (Section 3.1). Then we decompose this objective into a generative term that models the imprecise data distribution (Section 3.2) and a classification term that infers posterior label probabilities from imprecise supervision (Section 3.3). During generative modeling, we show that the imprecise-label conditional score can be expressed as a linear combination of clean-label conditional scores, weighted by the corresponding posterior probabilities. Building on this insight, we propose a weighted denoising score matching objective, which enables the model to achieve label-conditioned learning without requiring clean annotations. Finally, to reduce the time complexity of posterior inference, we further introduce an efficient timestep sampling strategy (Section 4). Extensive experiments across multiple tasks, including image generation, weakly supervised learning, and noisy dataset condensation show that CDMs trained with our framework not only achieve strong generative quality but also produce class-discriminative samples. Our contributions are summarized as follows:

- We propose a unified diffusion framework for training CDMs under diverse forms of imprecise supervision, which is the first exploration in the diffusion model field.
- To improve efficiency, we develop an optimized timestep sampling strategy for diffusion classifiers that greatly reduces the computation cost without compromising performance.
- Building on this framework, we pioneer the study of noisy dataset condensation, a practical yet previously unexplored setting, and establish a solid baseline for future research.
- Extensive experiments on image generation, weakly supervised learning, and noisy dataset condensation demonstrate the effectiveness and versatility of our unified framework.

## 2 BACKGROUND

**Diffusion Models.** Let  $\mathcal{X} \subseteq \mathbb{R}^d$  denote the  $d$ -dimensional input space. Given a clean input  $\mathbf{x} := \mathbf{x}_0$  from the real data distribution with density  $q(\mathbf{x}_0)$ , the forward diffusion process corrupts the data into a sequence of noisy samples  $\{\mathbf{x}_t\}_{t=1}^T$ <sup>1</sup> by gradually adding Gaussian noise with a fixed scaling schedule  $\{\alpha_t\}_{t=1}^T$  and a fixed noise schedule  $\{\sigma_t\}_{t=1}^T$ , as defined by

$$q(\mathbf{x}_t | \mathbf{x}_0) = \mathcal{N}(\mathbf{x}_t; \alpha_t \mathbf{x}_0, \sigma_t^2 \mathbf{I}), \quad (1)$$

where  $\mathbf{I}$  denotes the identity matrix and  $\mathcal{N}(\mathbf{x}; \boldsymbol{\mu}, \boldsymbol{\Sigma})$  denotes the Gaussian density with mean  $\boldsymbol{\mu}$  and covariance matrix  $\boldsymbol{\Sigma}$ . Assuming that the signal-to-noise ratio  $\text{SNR}(t) = \alpha_t^2 / \sigma_t^2$  decreases monotonically over time, the sample  $\mathbf{x}_t$  becomes increasingly noisier during the forward process. The scaling and noise schedules are prescribed such that  $\mathbf{x}_T$  nearly follows an isotropic Gaussian distribution. The reverse process for Eq. (1) is defined as a Markov chain, which aims to approximate  $q(\mathbf{x}_0)$  by gradually denoising from the standard Gaussian distribution  $p(\mathbf{x}_T) = \mathcal{N}(\mathbf{x}_T; \mathbf{0}, \mathbf{I})$ :

$$p_\theta(\mathbf{x}_{0:T}) = p(\mathbf{x}_T) \prod_{t=1}^T p_\theta(\mathbf{x}_{t-1} | \mathbf{x}_t), \quad (2)$$

$$p_\theta(\mathbf{x}_{t-1} | \mathbf{x}_t) = \mathcal{N}(\mathbf{x}_{t-1}; \boldsymbol{\mu}_\theta(\mathbf{x}_t, t), \tilde{\sigma}_t^2 \mathbf{I}), \quad (3)$$

where  $\boldsymbol{\mu}_\theta$  is generally parameterized by a time-conditioned score prediction network  $\mathbf{s}_\theta(\mathbf{x}_t, t)$  (Song et al., 2020; 2021; Song & Ermon, 2019; 2020):

$$\boldsymbol{\mu}_\theta(\mathbf{x}_t, t) = \frac{\alpha_{t-1}}{\alpha_t} \left[ \mathbf{x}_t + \left( \sigma_t^2 - \frac{\alpha_t^2}{\alpha_{t-1}^2} \sigma_{t-1}^2 \right) \mathbf{s}_\theta(\mathbf{x}_t, t) \right]. \quad (4)$$

The reverse process can be learned by optimizing the variational lower bound on log-likelihood as

$$\log p_\theta(\mathbf{x}) \geq -\mathbb{E}_t \left[ w_t \left\| \mathbf{s}_\theta(\mathbf{x}_t, t) - \nabla_{\mathbf{x}_t} \log q_t(\mathbf{x}_t) \right\|_2^2 \right] + C_1, \quad (5)$$

<sup>1</sup>We use the subscript  $t$  of the sample  $\mathbf{x}$  to denote the noisy version of the sample at timestep  $t$ .

where  $\mathbb{E}$  denotes the expectation,  $w_t = \frac{\sigma_t^2}{2} \left( \frac{\sigma_t^2 \alpha_{t-1}^2}{\sigma_{t-1}^2 \alpha_t^2} - 1 \right)$ , and  $C_1$  is a constant that is typically small and can be dropped (Song et al., 2020). The expectation term is called the *score matching loss* (Kingma et al., 2021), where  $\nabla \log q_t(\mathbf{x}_t)$  is the gradient of data density at  $\mathbf{x}_t$  in data space.

The above definition can be reformulated to match other commonly used diffusion models, such as those in Ho et al. (2020), Karras et al. (2022) and Song et al. (2020). The corresponding conversions are detailed in Appendix B.1. For clarity, we adopt the the elucidated diffusion model (EDM) (Karras et al., 2022) as the default diffusion model throughout this paper, as it offers a unified structure and well-optimized parameterization.

**Imprecise Supervision.** Imprecise-label data typically refers to settings where the true label is not directly available, and instead only imprecise label information is provided. Let  $\mathcal{Y} = [c] := \{1, \dots, c\}$  represent the label space with  $c$  distinct classes. In this work, we primarily focus on three representative forms of imprecise supervision that have been widely studied in the literature:

- *Partial-label data*, where each instance  $X$  is associated with a candidate label set  $S \subset [c]$  that is guaranteed to contain the true label  $Y$ , i.e.,  $p(Y \in S | X, S) = 1$ . This setting is widely studied in partial-label learning (Tian et al., 2023).
- *Supplementary-unlabeled data*, consisting of a small labeled subset  $(X^1, Y^1)$  together with a large number of unlabeled samples  $(X^u, \emptyset)$ . This scenario is the focus of semi-supervised learning (Yang et al., 2022), which aims to exploit unlabeled data to improve generalization.
- *Noisy-label data*, where the observed label  $\hat{Y}$  is a corrupted version of the underlying true label  $Y$ , modeled by a conditional distribution  $p(\hat{Y} | X, Y)$ . This gives rise to noisy-label learning (Han et al., 2020), which seeks to build models robust to label corruption.

### 3 METHODOLOGY

In this section, we first introduce the unified learning objective that integrates generative and classification components. Then we elaborate on the formulation and optimization of these components.

#### 3.1 UNIFIED LEARNING OBJECTIVE

To robustly learn a diffusion model with learnable parameters  $\theta$  under imprecise supervision (denoted as  $Z \subseteq \mathcal{Y}$ ), we treat the true label  $Y$  as a latent variable and maximize the likelihood of the joint distribution of the input  $X$  and  $Z$ . By the maximum likelihood principle, our objective is to find

$$\theta^* = \arg \max_{\theta} \log p_{\theta}(X, Z) = \arg \max_{\theta} \log \sum_{\mathcal{Y}} p_{\theta}(X, Y, Z), \quad (6)$$

where  $\theta^*$  denotes the optimal parameter. Eq. (6) involves the log of the marginalization over latent variables and cannot generally be solved in closed form. To circumvent this intractability, we instead maximize a variational lower bound on the marginal log-likelihood:

$$\begin{aligned} \theta^n &= \arg \max_{\theta} \mathbb{E}_{p_{\phi}(Y|X,Z)} [\log p_{\theta}(X, Y, Z)] \\ &= \arg \max_{\theta} \left\{ \log p_{\theta}(X | Z) + \mathbb{E}_{p_{\phi}(Y|X,Z)} [\log p_{\theta}(Y | X, Z)] \right\}, \end{aligned} \quad (7)$$

where  $\theta^n$  denotes the  $n$ -th estimate of  $\theta$ , and  $\phi$  is instantiated as the exponential moving average (EMA) of  $\theta$  over its 1st through  $(n-1)$  iterates. A complete derivation of this variational lower bound is provided in Appendix B.3. From Eq. (7), we can observe that maximizing the marginal likelihood can be performed from generative and classification perspectives. The former focuses on modeling the data distribution conditioned on the imprecise supervision, while the latter aims to infer the posterior distribution based on the feature and the imprecise label. In this paper, we adopt the commonly used class-conditional setting, where the generation of the imprecise label  $Z$  is assumed to be independent of the input  $X$  given the true label  $Y$  (Yao et al., 2020; Wen et al., 2021).

#### 3.2 GENERATIVE OBJECTIVE: MODELING THE IMPRECISE DATA DISTRIBUTION

Since samples are assumed to be independent of each other, we present the analysis in this and the following subsections using a single sample  $(\mathbf{x}, z)$  for notational clarity, with the final objective

computed over the entire dataset. Following the standard formulation of diffusion models in Eq. (5), we parameterize the conditional generative process  $p_\theta(\mathbf{x}|z)$  using a score network  $\mathbf{s}_\theta(\mathbf{x}_t, z, t)$ . The corresponding variational lower bound on the conditional log-likelihood is given by

$$\log p_\theta(\mathbf{x}_0|z) \geq -\mathbb{E}_t \left[ w_t \left\| \mathbf{s}_\theta(\mathbf{x}_t, z, t) - \nabla_{\mathbf{x}_t} \log q_{t|0}(\mathbf{x}_t | \mathbf{x}_0, z) \right\|_2^2 \right] + C_2, \quad (8)$$

where  $C_2$  is another constant. Directly optimizing the score network with this objective on imprecise-label data would lead it to converge to the score of the imprecise conditional distribution.

**Remark 1.** Let  $\hat{\theta}$  denote the parameters obtained by maximizing the lower bound in Eq. (8) using denoising score matching. In this case, the learned score function satisfies  $\mathbf{s}_{\hat{\theta}}(\mathbf{x}_t, z, t) = \nabla_{\mathbf{x}_t} \log q_t(\mathbf{x}_t | z)$  for all  $\mathbf{x}_t \in \mathcal{X}$ ,  $z \subseteq \mathcal{Y}$ , and  $t \in [T]$ . However, since  $q_t(\mathbf{x}_t | z)$  corresponds to the imprecise-label density, the resulting generation is biased and thus fails to fully recover the true data distribution. The derivation and visualization of this bias is deferred to Appendix B.5.

Therefore, to align the learned score with the clean-label conditional score, we propose modifying the objective to correct the gradient signal from score matching (Kingma et al., 2021). We begin by establishing the relationship between the imprecise-label and clean-label conditional scores.

**Theorem 1.** *Under the class-conditional setting, for all  $\mathbf{x}_t \in \mathcal{X}$ ,  $z \subseteq \mathcal{Y}$ , and  $t \in [T]$ ,*

$$\nabla_{\mathbf{x}_t} \log q_t(\mathbf{x}_t | z) = \sum_{y=1}^c p(y | \mathbf{x}_t, z) \nabla_{\mathbf{x}_t} \log q_t(\mathbf{x}_t | y). \quad (9)$$

The formal proof is in Appendix B.6. Since  $p(y | \mathbf{x}_t, z) \geq 0$  and  $\sum_{y=1}^c p(y | \mathbf{x}_t, z) = 1$ , Theorem 1 implies that the imprecise-label conditional score can be expressed as a convex combination of the clean-label conditional scores, weighted by  $p(y | \mathbf{x}_t, z)$ . These weights represent the model’s posterior probability over labels given  $\mathbf{x}_t$  and  $z$ , implicitly requiring the model to perform classification during training. To our knowledge, this is the first work to explicitly reveal and exploit the classification capability of diffusion models within the training process under imprecise supervision.

According to Remark 1, directly optimizing the denoising score matching objective in Eq. (8) drives the score network to approximate the imprecise-label conditional score. However, Theorem 1 shows that this score can be decomposed as a convex combination of clean-label conditional scores, weighted by the posterior probability  $p(y | \mathbf{x}_t, z)$ . Motivated by this insight, we propose a new training objective that supervises the clean-label score network  $\mathbf{s}_\theta(\mathbf{x}_t, y, t)$  through a reweighted aggregation of its posterior outputs. The resulting weighted denoising score matching loss is

$$\mathcal{L}_{\text{Gen}}(\theta) = \mathbb{E}_t \left[ w_t \left\| \sum_{y=1}^c p(y | \mathbf{x}_t, z) \mathbf{s}_\theta(\mathbf{x}_t, y, t) - \nabla_{\mathbf{x}_t} \log q_{t|0}(\mathbf{x}_t | \mathbf{x}_0, z) \right\|_2^2 \right]. \quad (10)$$

This loss encourages the weighted aggregation of clean-label scores to approximate the imprecise score derived from data, thereby enabling label-conditioned learning without the need for explicit clean annotations. The following Proposition 1, with proof provided in Appendix B.7, guarantees that the optimal solution recovers the clean-label conditional scores:

**Proposition 1.** *Let  $\theta_{\text{Gen}}^* = \arg \min_{\theta} \mathcal{L}_{\text{Gen}}(\theta)$  be the minimizer of Eq. (10). Then, for all  $\mathbf{x}_t \in \mathcal{X}$ ,  $z \subseteq \mathcal{Y}$ , and  $t \in [T]$ , the learned score function satisfies  $\mathbf{s}_{\theta_{\text{Gen}}^*}(\mathbf{x}_t, y, t) = \nabla_{\mathbf{x}_t} \log q_t(\mathbf{x}_t | y)$ .*

### 3.3 CLASSIFICATION OBJECTIVE: INFERRING LABELS FROM IMPRECISE SIGNALS

We assume the class prior to be uniform, i.e.,  $p(y) = 1/c$ . To infer the class-posterior probability  $p_\theta(y | \mathbf{x}_t)$ , we adopt a diffusion-based approximation as defined below:

**Definition 1** (Approximated Posterior Noised Diffusion Classifier (Chen et al., 2024b)). Assuming the uniform prior  $p(y)$ , the class-posterior probability for a noisy input  $\mathbf{x}_t$  under a conditional diffusion model can be derived using Bayes’ rule, as follows:

$$p_\theta(y | \mathbf{x}_t) = \frac{p_\theta(\mathbf{x}_t | y)}{\sum_{y'} p_\theta(\mathbf{x}_t | y')} = \frac{\exp\{\log p_\theta(\mathbf{x}_t | y)\}}{\sum_{y'} \exp\{\log p_\theta(\mathbf{x}_t | y')\}}. \quad (11)$$

Here, following Chen et al. (2024b), the conditional likelihood  $\log p_\theta(\mathbf{x}_t | y)$  is approximated by the conditional evidence lower bound (ELBO), given by

$$\log p_\theta(\mathbf{x}_t | y) \approx -\sum_{\tau=t+1}^{T-1} w_\tau \mathbb{E}_{q(\mathbf{x}_\tau | \mathbf{h}_\theta(\mathbf{x}_t, y, t))} \left[ \left\| \mathbf{h}_\theta(\mathbf{x}_\tau, y, \tau) - \mathbf{x}_0 \right\|_2^2 \right], \quad (12)$$

where  $\mathbf{h}_\theta(\mathbf{x}_\tau, y, \tau) = \frac{\mathbf{x}_\tau}{\alpha_\tau} + \frac{\sigma_\tau^2}{\alpha_\tau} \mathbf{s}_\theta(\mathbf{x}_\tau, y, \tau)$  and  $w_\tau = \frac{\sigma_\tau^2 + \sigma_{\text{data}}^2}{\sigma_\tau^2 \sigma_{\text{data}}^2} \cdot \frac{P_{\text{std}}^{-1}}{\sigma_\tau \sqrt{2\pi}} \exp\left\{-\frac{(\log \sigma_\tau - P_{\text{mean}})^2}{2P_{\text{std}}^2}\right\}$ .

This diffusion classifier can be extended to non-uniform priors by incorporating  $p(y)$  into the logits of class  $y$ , where  $p(y)$  is estimated from the training set (Luo et al., 2024; Wang et al., 2022a), as detailed in Appendix C.2. As training proceeds, the conditional ELBO converges towards the true distribution  $q_t(\mathbf{x}_t | y)$ , thereby yielding increasingly accurate posterior estimates. For convenience, we denote the class probability of a noisy input  $\mathbf{x}_t$  with the diffusion classifier as  $f(\mathbf{x}_t)$ .

To derive the classification loss, we transform the maximization problem of the classification term in Eq. (7) into the minimization of the negative log-likelihood. We show that the resulting objective, i.e.,  $-\sum_Y p_\phi(Y | X, Z) \log p_\theta(Y | X, Z)$ , naturally aligns closely with prior work (Lv et al., 2020; Tarvainen & Valpola, 2017; Liu et al., 2020) and has been shown to be effective in practice.

**Partial-label data.** For partial-label data, the imprecise label  $Z$  is given as a candidate set  $S$  that is guaranteed to include the true label. In this case, the posterior distribution  $p_\theta(Y | X, S)$  is restricted to assign non-zero probability only to labels within the candidate set. Accordingly, for each sample  $(\mathbf{x}, s)$ , we compute the classification loss from Eq. (7) as

$$\mathcal{L}_{\text{Cls}}^{\text{PL}}(\mathbf{x}) = -\sum_{y \in \mathcal{Y}} p_\phi(y | \mathbf{x}, s) \log p_\theta(y | \mathbf{x}, s) = -\sum_{y \in s} \tilde{f}_\phi(\mathbf{x})_y \log f_\theta(\mathbf{x})_y, \quad (13)$$

where  $\tilde{f}_\phi(\mathbf{x})$  denotes the normalized probability over  $s$  such that  $\sum_{y \in s} \tilde{f}_\phi(\mathbf{x})_y = 1$  and  $\tilde{f}_\phi(\mathbf{x})_y = 0$  for all  $y \notin s$ . Eq. (13) can be interpreted as an EMA-stabilized variant of the method called progressive identification (*PRODEN*) (Lv et al., 2020), where EMA predictions serve as soft pseudo-targets.

**Supplementary-unlabeled data.** In this scenario, the training set consists of a small portion of labeled data and a larger number of unlabeled data. This setting can be regarded as a special case of the partial-label formulation: labeled instances are assigned singleton candidate sets containing the ground-truth label, while unlabeled instances are associated with the full label space. Accordingly, the classification loss for each instance is defined as

$$\mathcal{L}_{\text{Cls}}^{\text{SU}}(\mathbf{x}) = -\sum_{y \in \mathcal{Y}} p_\phi(y | \mathbf{x}, z) \log p_\theta(y | \mathbf{x}, z) = -\sum_{y \in \mathcal{Y}} \tilde{f}_\phi(\mathbf{x})_y \log f_\theta(\mathbf{x})_y, \quad (14)$$

where  $\tilde{f}_\phi(\mathbf{x})$  denotes the pseudo-target distribution: for labeled samples, it reduces to a one-hot vector of the ground-truth label, while for unlabeled samples, it corresponds to the EMA model’s prediction over the entire label set. This loss can thus be viewed as an EMA-stabilized self-training objective (Tarvainen & Valpola, 2017), a widely used strategy in semi-supervised learning that leverages unlabeled data through soft pseudo-labels.

**Noisy-label data.** In practice, accurately distinguishing clean labels from noisy ones is often difficult, making it challenging to retain reliable supervision while applying self-training for label refinement. To mitigate this, we leverage the memorization effect in noisy-label learning, where neural networks typically fit clean labels before overfitting to noise (Han et al., 2020). Drawing inspiration from the noisy-label learning method called early learning regularization (*ELR*) (Liu et al., 2020), we propose a simpler yet effective loss function that retains its core idea, defined as

$$\mathcal{L}_{\text{Cls}}^{\text{NL}}(\mathbf{x}) = -\sum_{y \in \mathcal{Y}} \text{sg}(\mathbf{r}(\mathbf{x}))_y \log f_\theta(\mathbf{x})_y, \quad \mathbf{r}(\mathbf{x}) = \hat{\mathbf{y}} - \frac{f_\theta(\mathbf{x}) \odot (\langle f_\theta(\mathbf{x}), f_\phi(\mathbf{x}) \rangle \mathbf{1} - f_\phi(\mathbf{x}))}{1 - \langle f_\theta(\mathbf{x}), f_\phi(\mathbf{x}) \rangle}, \quad (15)$$

where  $\hat{\mathbf{y}}$  denotes the one-hot vector of the noisy label  $\hat{y}$ ,  $\text{sg}(\cdot)$  is the stop-gradient operator<sup>3</sup>,  $\odot$  is the Hadamard product, and  $\langle \cdot, \cdot \rangle$  denotes the inner product. This formulation inherits the core principle of *ELR*, stabilizing training through soft pseudo-targets derived from the EMA model. It effectively amplifies the gradient contribution of cleanly labeled samples while suppressing the influence of mislabeled ones, which we further analyze in detail in Appendix C.1.

## 4 TIME COMPLEXITY REDUCTION

The oracle diffusion classifier requires repeated calculations of the conditional ELBO across all classes to make a prediction, resulting in a substantial computation cost. To address this issue, Chen et al.

<sup>2</sup>As specified in the EDM (Karras et al., 2022), we use  $\sigma_{\text{data}} = 0.5$ ,  $P_{\text{mean}} = -1.2$  and  $P_{\text{std}} = 1.2$ .

<sup>3</sup>The stop-gradient operator  $\text{sg}(\cdot)$  returns its input but blocks gradient flow, i.e.,  $\nabla_{\mathbf{x}} \text{sg}(\mathbf{r}(\mathbf{x})) = 0$ .

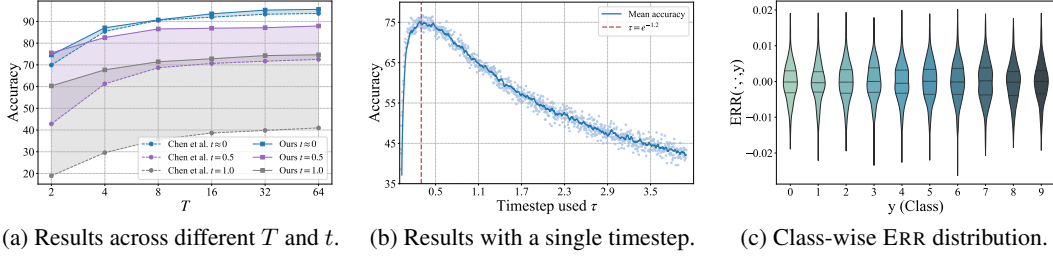


Figure 1: (a): Test accuracy (%) comparison on CIFAR-10 dataset under time complexity reduction technique from Chen et al. (2024c) and ours. (b): Test accuracy (%) on CIFAR-10 dataset evaluated with only a single timestep per class. (c): Violin plot of class-wise  $\text{ERR}(\cdot, \cdot, y)$  computed across samples using a fixed subinterval length  $\Delta$ . Wider regions of the violin indicate higher density.

(2024b) showed that when estimating ELBO with Monte Carlo sampling, reusing the same  $\mathbf{x}_\tau$  across classes and selecting timesteps at uniform intervals is sufficient for effective classification. However, our experiments reveal that this strategy is empirically suboptimal as illustrated in Figure 1(a). We identify the core reason to be the model’s varying discriminative ability across different timesteps, with notable disparities in performance, as shown in Figure 1(b) where the accuracy is evaluated using only a single timestep. Specifically, when the timestep  $\tau$  is small, the added noise is negligible, leading to reconstructions with low label sensitivity. Conversely, when the timestep  $\tau$  is large, the input becomes overwhelmed by noise, rendering the predictions highly unreliable.

To this end, we aim to identify a compact subset of timesteps that enables efficient ELBO estimation while maintaining sufficient classification performance. Let  $p(\tau)$  be a probability density function over the interval  $\tau \in (0, +\infty)$ , satisfying  $\int_0^{+\infty} p(\tau) d\tau = 1$ . Our objective is to select a subinterval  $\tau \in [l, r]$  such that

$$\underset{0 \leq l \leq r}{\text{minimize}} \left\| \mathbb{E}_{\tau \sim p(\tau) | \tau \in [l, r]} [\hat{h}(\tau, y)] - \mathbb{E}_{\tau \sim p(\tau)} [\hat{h}(\tau, y)] \right\|_2^2, \quad (16)$$

where  $\hat{h}(\tau, y) = w_\tau \mathbb{E}_{\mathbf{x}_\tau} [\| \mathbf{h}_\theta(\mathbf{x}_\tau, y, \tau) - \mathbf{x}_0 \|_2^2]$ . Eq. (16) formalizes the goal of finding a representative range where the expected reconstruction error closely matches that of the full distribution. To strike a compromise between signal and noise within the selected subinterval, we propose choosing it around the median of  $p(\tau)$ , so that signal-dominant early timesteps and noise-dominant later timesteps complement each other. This strategy yields a more stable and representative approximation, especially when  $p(\tau)$  is skewed. Therefore, we provide a formal characterization of the subinterval construction for the EDM by the following theorem.

**Theorem 2.** Consider an EDM where  $\tau$  is sampled from a log-normal distribution, i.e.,  $\ln(\tau) \sim \mathcal{N}(\tau; P_{\text{mean}}, P_{\text{std}}^2)$ , where  $P_{\text{mean}} \in \mathbb{R}$  and  $P_{\text{std}} > 0$ . Given a fixed subinterval length  $\Delta$ , a sampling range centered around the median of  $p(\tau)$  can be constructed by solving the following equation for the left boundary  $l$ :

$$l = \text{Solve}_\tau (F(\tau) + F(\tau + \Delta) - 1 = 0), \quad r = l + \Delta,$$

where  $\text{Solve}_\tau(\cdot)$  denotes a numerical root-finding algorithm over  $\tau$ , such as the Brent method (Brent, 2013), and  $F(\cdot)$  is the cumulative distribution function of  $p(\tau)$ .

The proof of Theorem 2 as well as a similar conclusion for denoising diffusion probabilistic model (DDPM) (Ho et al., 2020) are provided in Appendix B.8. Notably, our finding aligns with the effective timestep hypothesis proposed in Li et al. (2023) for the DDPM setting. Furthermore, based on Eq. (16), we can derive a necessary condition that any theoretically optimal subinterval must satisfy, as formalized in the following theorem:

**Theorem 3 (Necessary Condition for Optimal Subinterval).** Given  $(l^*, r^*)$  be an optimal subinterval of the support of  $p(\tau)$ , a necessary condition for attaining the theoretical minimum of the squared error objective in Eq. (16) is

$$\text{ERR}(l^*, r^*, y) = \mathbb{E}_{\tau \sim p(\tau) | \tau \in [l^*, r^*]} [\hat{h}(\tau, y)] - \frac{\hat{h}(l^*, y) + \hat{h}(r^*, y)}{2} = 0. \quad (17)$$

Table 1: Generative results on CIFAR-10 and ImageNette under various settings. ‘uncond’ and ‘cond’ indicate unconditional and conditional metrics. **Bold** numbers indicate better performance.

Metric			Noisy-label supervision				Partial-label supervision				Suppl-unlabeled supervision			
			Sym-40%		Asym-40%		Random		Class-50%		Random-1%		Random-10%	
			Vanilla	DMIS	Vanilla	DMIS	Vanilla	DMIS	Vanilla	DMIS	Vanilla	DMIS	Vanilla	DMIS
CIFAR-10	uncond	FID	(↓) <b>3.33</b>	3.47	3.23	<b>3.10</b>	7.76	<b>2.26</b>	11.75	<b>2.77</b>	3.16	<b>3.12</b>	2.93	<b>2.89</b>
		IS	(↑) 9.56	<b>9.68</b>	9.02	<b>9.73</b>	9.09	<b>9.80</b>	9.62	<b>9.68</b>	10.03	<b>10.57</b>	9.80	<b>9.83</b>
		Density Coverage	(↑) 101.39	<b>109.75</b>	100.06	<b>109.69</b>	103.21	<b>106.49</b>	108.76	<b>109.06</b>	97.19	<b>108.18</b>	99.96	<b>108.87</b>
	cond	CW-FID	(↓) 29.84	<b>13.85</b>	14.70	<b>13.24</b>	27.18	<b>10.65</b>	32.44	<b>11.56</b>	16.25	<b>16.12</b>	11.84	<b>11.77</b>
		CW-Density	(↑) 72.98	<b>107.23</b>	90.85	<b>107.07</b>	102.04	<b>105.75</b>	102.43	<b>108.66</b>	89.99	<b>100.73</b>	96.29	<b>107.94</b>
		CW-Coverage	(↑) 73.39	<b>80.11</b>	79.63	<b>79.65</b>	65.45	<b>82.09</b>	61.45	<b>81.24</b>	75.03	<b>76.84</b>	80.80	<b>81.12</b>
ImageNette	uncond	FID	(↓) 14.11	<b>13.44</b>	13.93	<b>13.91</b>	79.13	<b>72.62</b>	91.28	<b>79.12</b>	23.88	<b>19.26</b>	14.32	<b>12.84</b>
		IS	(↑) 12.69	<b>13.21</b>	12.51	<b>13.73</b>	9.19	<b>9.40</b>	<b>9.27</b>	9.11	12.23	<b>13.72</b>	12.80	<b>13.16</b>
		Density Coverage	(↑) 109.31	<b>112.52</b>	<b>111.66</b>	106.78	95.33	<b>99.83</b>	94.29	<b>102.58</b>	115.94	<b>125.68</b>	105.27	<b>109.23</b>
	cond	CW-FID	(↓) 80.31	<b>60.12</b>	62.26	<b>58.20</b>	157.76	<b>63.58</b>	163.45	<b>67.92</b>	71.66	<b>70.27</b>	49.22	<b>44.31</b>
		CW-Density	(↑) 73.99	<b>81.12</b>	93.53	<b>94.58</b>	93.38	<b>95.83</b>	91.50	<b>95.21</b>	115.90	<b>118.69</b>	103.41	<b>115.67</b>
		CW-Coverage	(↑) 67.89	<b>71.94</b>	74.18	<b>75.82</b>	19.76	<b>24.35</b>	15.88	<b>18.93</b>	51.73	<b>52.15</b>	72.61	<b>74.85</b>

The proof of Theorem 3 can be found in Appendix B.9. Based on Theorem 3, we empirically present the class-wise distribution of  $\text{ERR}(\cdot, \cdot, y)$  across samples in Figure 1(c), where the errors are generally concentrated around zero, supporting the effectiveness of our proposed time complexity reduction strategy. Notably, when the subinterval is reduced to a single sampling point, choosing the median of  $p(\tau)$  (i.e.,  $e^{\tau_{\text{mean}}}$ ) yields the best classification performance as shown in Figure 1(b). This observation is consistent with our earlier hypothesis regarding the informativeness of the median timestep. In practical posterior inference, we combine timestep subinterval reduction strategy with  $\mathbf{x}_\tau$  reuse technique (Chen et al., 2024c) to further improve inference efficiency.

## 5 EXPERIMENTS

We present experiments on three tasks including image generation, weakly supervised learning, and dataset condensation to demonstrate the utility and versatility of our method. Evaluations are performed on three benchmark datasets widely used for both generation and classification, covering image resolutions from  $28 \times 28$  (Fashion-MNIST (Xiao et al., 2017)) and  $32 \times 32$  (CIFAR-10 (Krizhevsky et al., 2009)) to  $64 \times 64$  (ImageNette (Deng et al., 2009)). As a baseline, we refer to the model trained with the generative objective in Eq. (8) as the *Vanilla* method. The training hyperparameters are kept consistent with those used in the EDM model (Karras et al., 2022).

**Dataset construction.** For partial-label data, we generate synthetic candidate label sets using both class-dependent (Wen et al., 2021) and random generation models (Feng et al., 2020). In the class-dependent setting, we construct a transition matrix that maps each true label to a set of semantically similar labels, where each similar label is included in the candidate set with probability 50%. In contrast, the random setting assign each incorrect label an equal probability 50% of being included in the candidate set. For supplementary-unlabeled data, we follow a standard semi-supervised setup by randomly selecting 10% and 1% of the training data classwise as labeled samples, and treating the remaining data as unlabeled. For noisy-label data, we consider both symmetric and asymmetric noise. In the symmetric case, labels are uniformly flipped to any incorrect class, whereas in the asymmetric case, they are flipped to semantically similar classes according to a predefined mapping. In both cases, the corruption probability is referred to as the noise rate, which is set to 40%.

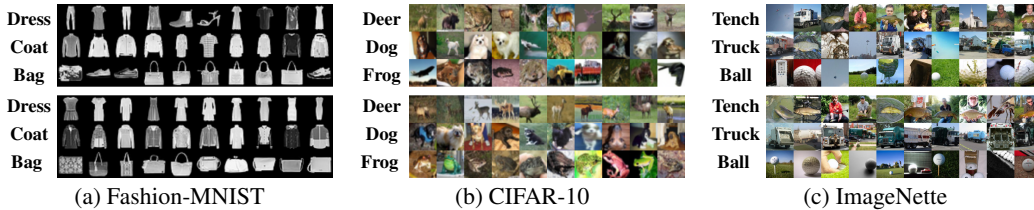
Figure 2: Comparison of conditionally generated images from *Vanilla* (top) and our *DMIS* model (bottom), each trained with 40% symmetric noise on Fashion-MNIST, CIFAR-10, and ImageNette.

Table 2: Classification results (test accuracy, %) on Fashion-MNIST, CIFAR-10, and ImageNette datasets under various types of imprecise supervision ( $\spadesuit$ : partial-label,  $\heartsuit$ : supplementary-unlabeled,  $\clubsuit$ : noisy-label). **Bold** numbers indicate the best performance.<sup>5</sup>

Dataset $\spadesuit$	Type	<i>PRODEN</i>	<i>IDGP</i>	<i>PiCO</i>	<i>CRDPLL</i>	<i>DIRK</i>	<i>Vanilla</i>	<i>DMIS<sup>CE</sup></i>	<i>DMIS</i>
F-MNIST	Random	93.31±0.07	92.26±0.25	93.32±0.12	94.03±0.14	94.11±0.22	80.20±1.29	84.24±0.37	<b>94.27±0.55</b>
	Class-50%	93.44±0.21	93.07±0.16	93.32±0.33	93.80±0.23	93.99±0.24	66.03±1.43	78.45±0.46	<b>94.20±0.15</b>
CIFAR-10	Random	90.02±0.22	89.65±0.53	86.40±0.89	92.74±0.26	93.48±0.14	60.25±0.17	91.47±0.15	<b>94.70±0.49</b>
	Class-50%	90.44±0.44	90.83±0.34	87.51±0.66	92.89±0.27	93.22±0.37	56.34±0.50	90.52±0.33	<b>93.53±0.12</b>
ImageNette	Random	84.75±0.13	84.07±0.26	82.15±0.23	84.31±0.25	87.90±0.11	56.04±0.61	84.49±0.05	<b>89.31±0.21</b>
	Class-50%	83.50±0.60	82.18±0.13	84.41±0.93	88.08±0.34	87.47±0.17	59.47±0.51	82.34±0.27	<b>88.42±0.43</b>
Dataset $\heartsuit$	Type	<i>Dash</i>	<i>CoMatch</i>	<i>FlexMatch</i>	<i>SimMatch</i>	<i>SoftMatch</i>	<i>Vanilla</i>	<i>DMIS<sup>CE</sup></i>	<i>DMIS</i>
F-MNIST	Random-1%	84.73±0.09	85.31±0.29	84.43±0.30	84.69±0.17	84.72±0.23	78.37±0.72	82.92±0.17	<b>85.92±0.13</b>
	Random-10%	91.16±0.20	90.52±0.12	90.69±0.03	91.18±0.13	91.22±0.11	90.50±1.00	91.07±0.18	<b>92.97±0.21</b>
CIFAR-10	Random-1%	70.14±0.69	61.45±1.46	70.72±0.93	73.33±1.02	73.74±0.82	53.49±0.15	75.30±0.17	<b>76.40±0.54</b>
	Random-10%	81.50±0.68	77.79±0.53	81.35±0.48	82.90±0.43	88.66±0.60	85.13±0.12	89.85±0.08	<b>92.47±0.39</b>
ImageNette	Random-1%	57.68±2.19	63.88±0.78	61.39±0.70	58.12±2.66	58.50±2.31	49.55±0.99	62.64±0.24	<b>68.23±0.19</b>
	Random-10%	74.66±0.81	73.20±0.46	73.08±0.13	75.12±0.45	75.75±0.25	74.70±0.53	71.39±0.45	<b>77.30±0.15</b>
Dataset $\clubsuit$	Type	<i>CE</i>	<i>Mixup</i>	<i>Coteaching</i>	<i>ELR</i>	<i>PENCIL</i>	<i>Vanilla</i>	<i>DMIS<sup>CE</sup></i>	<i>DMIS</i>
F-MNIST	Sym-40%	76.18±0.26	92.21±0.03	92.17±0.34	93.13±0.13	90.85±0.58	90.11±1.24	87.76±0.57	<b>93.40±0.40</b>
	Asym-40%	82.01±0.06	92.01±1.02	92.78±0.25	92.82±0.09	91.77±0.69	85.41±0.96	83.39±0.24	<b>93.20±0.30</b>
CIFAR-10	Sym-40%	67.22±0.26	84.26±0.64	86.54±0.57	85.68±0.13	85.91±0.26	80.22±0.10	84.75±0.36	<b>88.63±0.12</b>
	Asym-40%	76.98±0.42	83.21±0.85	79.38±0.39	81.32±0.31	84.89±0.49	86.31±0.10	84.21±0.18	<b>88.83±0.33</b>
ImageNette	Sym-40%	58.43±0.77	76.65±1.62	66.55±1.00	84.33±2.86	81.94±1.26	55.86±1.95	80.47±0.56	<b>84.12±0.18</b>
	Asym-40%	71.81±0.38	77.16±0.71	75.12±0.50	73.51±0.31	77.20±1.15	53.91±1.07	77.21±0.19	<b>79.30±0.27</b>

## 5.1 TASK1: IMAGE GENERATION

**Setup.** We evaluate the trained CDMs using four unconditional metrics, including Fréchet Inception Distance (FID) (Heusel et al., 2017), Inception Score (IS) (Salimans et al., 2016), Density, and Coverage (Naeem et al., 2020), as well as three conditional metrics, namely CW-FID, CW-Density, and CW-Coverage (Chao et al., 2022). The Class-Wise (CW) metrics are computed per class and then averaged. Detailed descriptions of these metrics are provided in the Appendix E.1.

**Results.** Table 1 reports the generative performance of the *Vanilla* model and our proposed *DMIS* model on various settings. It can be seen that our model outperforms the baseline across almost all cases with respect to both unconditional and conditional metrics. The performance gap is especially pronounced under partial-label supervision. These results indicate that *DMIS* not only enhances the quality of samples but also produces generative distributions that more closely align with the true data distribution. Furthermore, Figure 2 compares conditionally generated samples from the *Vanilla* and *DMIS* models across different datasets. Compared to the *Vanilla* model which often produces samples misaligned with the class, our model produces images of higher visual fidelity and class-conditional generations that more accurately reflect the intended semantic categories.

## 5.2 TASK2: WEAKLY SUPERVISED LEARNING

**Setup.** We evaluate our method under three weakly supervised scenarios. In partial-label learning, we compare against approaches including *PRODEN* (Lv et al., 2020), *IDGP* (Qiao et al., 2023), *PiCO* (Wang et al., 2023), *CRDPLL* (Wu et al., 2022) and *DIRK* (Wu et al., 2024). For semi-supervised learning, we adopt *Dash* (Xu et al., 2021), *CoMatch* (Li et al., 2021a), *FlexMatch* (Zhang et al., 2021a), *SimMatch* (Zheng et al., 2022) and *SoftMatch* (Chen et al., 2023) as comparison methods. For noisy-label learning, we compare with *Coteaching* (Han et al., 2018), *ELR* (Liu et al., 2020), *PENCIL* (Yi & Wu, 2019), as well as standard normal cross-entropy (*CE*) training and *Mixup* (Zhang et al., 2018). To ensure a fair comparison, the discriminative classifier is implemented as Wide-ResNet-40-10 with 55.84M parameters, while our generative model contains 55.73M parameters, and all models are trained from scratch without pre-training.

**Results.** The classification results for weakly supervised learning are reported in Table 2. Overall, our method *DMIS*, evaluated via a diffusion classifier, achieves the best performance, demonstrating the stronger generalization capability of diffusion models over prior discriminative approaches. Interestingly, the *Vanilla* method still outperforms several baselines, particularly in the noisy-label setting, suggesting that the vanilla denoising score matching objective still acts as an implicit regularizer

<sup>5</sup>*DMIS<sup>CE</sup>* denotes regenerate-classification results, i.e., we regenerate datasets of the same size under conditional sampling and then train a discriminative model on them using standard *CE* loss.

Table 3: Classification results (test accuracy, %) on noisy-label Fashion-MNIST, CIFAR-10, and ImageNette datasets. ‘IPC’ indicates the number of images per class in the condensed dataset. **Bold numbers indicate the best performance.**

Dataset	Type	IPC	Random	DC	DSA	DM	MTT	RDED	SRE2L	DMIS
F-MNIST	Sym-40%	10	34.42±0.69	22.85±1.69	42.07±2.49	57.06±1.52	9.03±3.81	18.57±1.06	15.80±0.38	<b>70.18±0.37</b>
		50	52.36±0.60	35.64±2.26	55.22±1.51	68.23±0.47	10.91±0.82	23.19±0.74	19.51±0.96	<b>80.73±0.07</b>
		100	55.14±0.06	30.46±1.74	41.30±0.85	73.21±0.69	13.73±3.96	25.43±0.21	19.66±1.91	<b>84.26±0.02</b>
	Asym-40%	10	48.28±0.34	53.17±1.59	57.15±2.37	63.27±1.60	8.75±0.82	18.42±1.62	16.45±1.96	<b>65.02±1.85</b>
		50	69.44±0.17	49.21±0.69	77.20±0.34	76.39±0.57	8.76±2.11	22.31±0.67	27.07±0.35	<b>79.65±0.63</b>
		100	70.80±0.91	36.95±0.57	80.24±0.54	78.43±0.63	12.59±1.22	24.03±0.97	26.52±1.46	<b>83.22±0.33</b>
CIFAR-10	Sym-40%	10	16.30±0.96	18.11±1.02	18.06±1.72	23.71±0.40	12.06±0.46	19.85±0.88	13.12±1.04	<b>27.83±0.98</b>
		50	26.59±0.70	20.63±0.22	28.76±0.57	29.50±0.56	17.96±2.10	34.64±0.58	14.23±1.67	<b>46.47±0.41</b>
		100	31.19±0.74	19.91±0.54	29.45±0.34	32.26±0.75	18.04±3.55	44.03±0.21	14.21±0.93	<b>56.53±0.03</b>
	Asym-40%	10	24.89±1.65	18.51±1.35	22.23±1.80	26.53±0.07	9.62±1.45	23.48±0.65	14.64±1.03	<b>24.94±0.49</b>
		50	40.95±0.59	25.97±0.97	40.81±0.29	43.09±0.76	16.54±1.88	39.12±0.13	16.03±0.21	<b>47.77±0.78</b>
		100	47.49±0.64	27.76±0.72	42.96±0.84	51.61±0.60	17.67±2.53	44.45±0.19	17.55±0.91	<b>55.89±0.39</b>
ImageNette	Sym-40%	10	23.09±0.19	15.89±0.73	27.70±1.25	28.83±0.73	33.60±0.53	21.15±1.05	25.03±1.17	<b>34.36±1.05</b>
		50	33.83±0.28	24.62±0.73	32.07±1.01	42.66±1.27	38.39±1.67	35.87±0.39	35.37±0.82	<b>44.93±0.28</b>
		100	40.04±0.71	22.81±1.22	36.05±1.76	43.25±2.13	39.61±1.52	35.87±0.39	41.74±1.37	<b>56.23±0.84</b>
	Asym-40%	10	26.54±0.88	19.26±0.98	30.62±2.09	33.40±0.48	33.65±1.29	26.23±0.06	25.74±2.21	<b>37.09±0.29</b>
		50	47.91±0.61	31.68±2.15	43.41±1.24	50.97±1.61	38.71±1.24	32.75±0.43	35.29±0.14	<b>55.20±0.46</b>
		100	59.10±1.41	29.19±0.21	53.79±0.84	60.70±1.88	37.69±1.29	35.48±0.22	42.37±0.34	<b>68.97±1.12</b>

against label noise. Moreover, compared to standard *CE* training, the regenerate-classification variant *DMIS*<sup>CE</sup> improves accuracy by up to 11.58%, 17.53%, and 22.13% on Fashion-MNIST, CIFAR-10, and ImageNette dataset, respectively, showing that the regenerated dataset effectively mitigates label imprecision and yields cleaner supervision for downstream discriminative training.

### 5.3 TASK3: NOISY DATASET CONDENSATION

While the task of dataset condensation has achieved remarkable progress recently, existing methods are typically developed under the assumption of clean labels. However, label noise is inevitable and cannot be fully eliminated in practice. Therefore, exploring how to condense a clean dataset from noisy-label data is natural and meaningful. To the best of our knowledge, this is the first work to investigate dataset condensation under noisy supervision, which we term *noisy dataset condensation*.

**Setup.** During condensation, we employ our trained CDMs to synthesize images according to the specified IPC. For evaluation, we compare against both hard-label-based methods, including *DC* (Zhao et al., 2021), *DSA* (Zhao & Bilen, 2021), *DM* (Zhao & Bilen, 2023), and *MTT* (Cazenavette et al., 2022b), as well as soft-label-based methods, namely *RDED* (Sun et al., 2024) and *SRE2L* (Yin et al., 2024). Following common protocols (Sun et al., 2024; Yin et al., 2024), we adopt ResNet-18 as the backbone during condensation and evaluate the condensed datasets on a test set using ResNet-34.

**Results.** Table 3 presents the results of noisy dataset condensation, with qualitative visualizations provided in Appendix E.5. Our method consistently surpasses prior approaches across datasets and noise types. These results highlight the advantage of generative condensation: rather than memorizing noisy labels, *DMIS* implicitly denoises them during generation, leading to cleaner condensed datasets. Notably, unlike the trends observed in clean dataset condensation, distribution-matching methods (e.g., *DM*) achieve the second-best results in this noisy setting, suggesting that distribution alignment helps regularize the effect of label noise. Moreover, instance-selection methods generally outperform synthetic-generation methods (e.g., *Random* vs. *DC/DSA/MTT* and *RDED* vs. *SRE2L*), indicating that discarding noisy samples during condensation is also an effective strategy to mitigate label noise. Collectively, these findings not only demonstrate the superiority of our approach but also provide useful insights for future work on noisy dataset condensation.

## 6 CONCLUSION

In this paper, we addressed the challenge of training CDMs under imprecise supervision, a setting that frequently arises in real-world applications. We introduced a unified framework that formulates the learning problem as likelihood maximization and decomposes it into generative and classification components. Based on this formulation, we proposed a weighted denoising score matching objective that enables label-conditioned learning without clean annotations, and developed an efficient timestep sampling strategy to reduce the computational cost of posterior inference. Extensive experiments across image generation, weakly supervised learning, and noisy dataset condensation verified the

effectiveness and versatility of our approach. Beyond establishing strong baselines, our work also pioneers the study of noisy dataset condensation, opening new opportunities for future exploration in robust and scalable diffusion modeling under weak supervision.

## REFERENCES

- David Berthelot, Nicholas Carlini, Ekin D Cubuk, Alex Kurakin, Kihyuk Sohn, Han Zhang, and Colin Raffel. Remixmatch: Semi-supervised learning with distribution matching and augmentation anchoring. In *International Conference on Learning Representations*, 2019a.
- David Berthelot, Nicholas Carlini, Ian Goodfellow, Nicolas Papernot, Avital Oliver, and Colin A Raffel. Mixmatch: A holistic approach to semi-supervised learning. In *Advances in Neural Information Processing Systems*, pp. 5050–5060, 2019b.
- Richard P Brent. *Algorithms for minimization without derivatives*. Courier Corporation, 2013.
- George Cazenavette, Tongzhou Wang, Antonio Torralba, Alexei A Efros, and Jun-Yan Zhu. Dataset distillation by matching training trajectories. In *IEEE/CVF Conference on Computer Vision and Pattern Recognition*, pp. 4750–4759, 2022a.
- George Cazenavette, Tongzhou Wang, Antonio Torralba, Alexei A Efros, and Jun-Yan Zhu. Dataset distillation by matching training trajectories. In *IEEE/CVF Conference on Computer Vision and Pattern Recognition*, pp. 4750–4759, 2022b.
- Chen-Hao Chao, Wei-Fang Sun, Bo-Wun Cheng, Yi-Chen Lo, Chia-Che Chang, Yu-Lun Liu, Yu-Lin Chang, Chia-Ping Chen, and Chun-Yi Lee. Denoising likelihood score matching for conditional score-based data generation. In *International Conference on Learning Representations*, 2022.
- Hao Chen, Ran Tao, Yue Fan, Yidong Wang, Jindong Wang, Bernt Schiele, Xing Xie, Bhiksha Raj, and Marios Savvides. Softmatch: Addressing the quantity-quality tradeoff in semi-supervised learning. In *International Conference on Learning Representations*, 2023.
- Hao Chen, Ankit Shah, Jindong Wang, Ran Tao, Yidong Wang, Xiang Li, Xing Xie, Masashi Sugiyama, Rita Singh, and Bhiksha Raj. Imprecise label learning: A unified framework for learning with various imprecise label configurations. In *Advances in Neural Information Processing Systems*, pp. 59621–59654, 2024a.
- Huanran Chen, Yinpeng Dong, Shitong Shao, Zhongkai Hao, Xiao Yang, Hang Su, and Jun Zhu. Diffusion models are certifiably robust classifiers. In *Advances in Neural Information Processing Systems*, pp. 50062–50097, 2024b.
- Huanran Chen, Yinpeng Dong, Zhengyi Wang, Xiao Yang, Chengqi Duan, Hang Su, and Jun Zhu. Robust classification via a single diffusion model. In *Proceedings of the International Conference on Machine Learning*, pp. 6643–6665, 2024c.
- Ciprian Corneanu, Raghudeep Gadde, and Aleix M Martinez. Latentpaint: Image inpainting in latent space with diffusion models. In *Proceedings of the IEEE/CVF winter conference on applications of computer vision*, pp. 4334–4343, 2024.
- Justin Cui, Ruochen Wang, Si Si, and Cho-Jui Hsieh. Scaling up dataset distillation to imagenet-1k with constant memory. In *Proceedings of the International Conference on Machine Learning*, pp. 6565–6590, 2023.
- Jia Deng, Wei Dong, Richard Socher, Li-Jia Li, Kai Li, and Li Fei-Fei. Imagenet: A large-scale hierarchical image database. In *IEEE/CVF Conference on Computer Vision and Pattern Recognition*, pp. 248–255, 2009.
- Prafulla Dhariwal and AlexanderQuinn Nichol. Diffusion models beat gans on image synthesis. In *Advances in Neural Information Processing Systems*, pp. 8780–8794, 2021.
- Bradley Efron. Tweedie’s formula and selection bias. *Journal of the American Statistical Association*, pp. 1602–1614, 2011.

- Patrick Esser, Sumith Kulal, Andreas Blattmann, Rahim Entezari, Jonas Müller, Harry Saini, Yam Levi, Dominik Lorenz, Axel Sauer, Frederic Boesel, et al. Scaling rectified flow transformers for high-resolution image synthesis. In *Proceedings of the International Conference on Machine Learning*, pp. 12606–12633, 2024.
- Lei Feng, Jiaqi Lv, Bo Han, Miao Xu, Gang Niu, Xin Geng, Bo An, and Masashi Sugiyama. Provably consistent partial-label learning. In *Advances in Neural Information Processing Systems*, pp. 10948–10960, 2020.
- Josh Givens, Song Liu, and Henry Reeve. Score matching with missing data. In *Proceedings of the International Conference on Machine Learning*, 2025.
- Jacob Goldberger and Ehud Ben-Reuven. Training deep neural-networks using a noise adaptation layer. In *International Conference on Learning Representations*, 2017.
- Ziyao Guo, Kai Wang, George Cazenavette, Hui Li, Kaipeng Zhang, and Yang You. Towards lossless dataset distillation via difficulty-aligned trajectory matching. In *International Conference on Learning Representations*, 2024.
- Bo Han, Quanming Yao, Xingrui Yu, Gang Niu, Miao Xu, Weihua Hu, Ivor Tsang, and Masashi Sugiyama. Co-teaching: Robust training of deep neural networks with extremely noisy labels. In *Advances in Neural Information Processing Systems*, pp. 8536–8546, 2018.
- Bo Han, Quanming Yao, Tongliang Liu, Gang Niu, Ivor W Tsang, James T Kwok, and Masashi Sugiyama. A survey of label-noise representation learning: Past, present and future. *arXiv preprint arXiv:2011.04406*, 2020.
- Chunming He, Chengyu Fang, Yulun Zhang, Longxiang Tang, Jinfa Huang, Kai Li, Zhenhua Guo, Xiu Li, and Sina Farsiu. Reti-diff: Illumination degradation image restoration with retinex-based latent diffusion model. In *International Conference on Learning Representations*, 2025.
- Wei He, Kai Han, Ying Nie, Chengcheng Wang, and Yunhe Wang. Species196: A one-million semi-supervised dataset for fine-grained species recognition. In *Advances in Neural Information Processing Systems*, pp. 44957–44975, 2023.
- Yang He, Lingao Xiao, Joey Tianyi Zhou, and Ivor Tsang. Multisize dataset condensation. In *International Conference on Learning Representations*, 2024.
- Martin Heusel, Hubert Ramsauer, Thomas Unterthiner, Bernhard Nessler, and Sepp Hochreiter. Gans trained by a two time-scale update rule converge to a local nash equilibrium. In *Advances in Neural Information Processing Systems*, pp. 6626–6637, 2017.
- Jonathan Ho and Tim Salimans. Classifier-free diffusion guidance. In *NeurIPS 2021 Workshop on Deep Generative Models and Downstream Applications*, 2022.
- Jonathan Ho, Ajay Jain, and Pieter Abbeel. Denoising diffusion probabilistic models. In *Advances in Neural Information Processing Systems*, pp. 6840–6851, 2020.
- Jonathan Ho, Tim Salimans, Alexey Gritsenko, William Chan, Mohammad Norouzi, and David J Fleet. Video diffusion models. In *Advances in Neural Information Processing Systems*, pp. 8633–8646, 2022.
- Takuhiro Kaneko, Yoshitaka Ushiku, and Tatsuya Harada. Label-noise robust generative adversarial networks. In *IEEE/CVF Conference on Computer Vision and Pattern Recognition*, pp. 2467–2476, 2019.
- Tero Karras, Miika Aittala, Timo Aila, and Samuli Laine. Elucidating the design space of diffusion-based generative models. In *Advances in Neural Information Processing Systems*, pp. 26565–26577, 2022.
- Jang-Hyun Kim, Jinuk Kim, Seong Joon Oh, Sangdoon Yun, Hwanjun Song, Joonhyun Jeong, Jung-Woo Ha, and Hyun Oh Song. Dataset condensation via efficient synthetic-data parameterization. In *Proceedings of the International Conference on Machine Learning*, pp. 11102–11118, 2022.

- Diederik Kingma, Tim Salimans, Ben Poole, and Jonathan Ho. Variational diffusion models. In *Advances in Neural Information Processing Systems*, pp. 21696–21707, 2021.
- Alex Krizhevsky, Geoffrey Hinton, et al. Learning multiple layers of features from tiny images. 2009.
- Dong-Hyun Lee et al. Pseudo-label: The simple and efficient semi-supervised learning method for deep neural networks. In *Workshop on challenges in representation learning, ICML*, pp. 896, 2013.
- Saehyung Lee, Sanghyuk Chun, Sangwon Jung, Sangdoon Yun, and Sungroh Yoon. Dataset condensation with contrastive signals. In *Proceedings of the International Conference on Machine Learning*, pp. 12352–12364, 2022.
- Alexander C Li, Mihir Prabhudesai, Shivam Duggal, Ellis Brown, and Deepak Pathak. Your diffusion model is secretly a zero-shot classifier. In *Proceedings of the IEEE/CVF International Conference on Computer Vision*, pp. 2206–2217, 2023.
- Junnan Li, Caiming Xiong, and Steven CH Hoi. Comatch: Semi-supervised learning with contrastive graph regularization. In *Proceedings of the IEEE/CVF International Conference on Computer Vision*, pp. 9475–9484, 2021a.
- Wen Li, Limin Wang, Wei Li, Eirikur Agustsson, and Luc Van Gool. Webvision database: Visual learning and understanding from web data. *arXiv preprint arXiv:1708.02862*, 2017.
- Xuefeng Li, Tongliang Liu, Bo Han, Gang Niu, and Masashi Sugiyama. Provably end-to-end label-noise learning without anchor points. In *Proceedings of the International Conference on Machine Learning*, pp. 6403–6413, 2021b.
- Yangming Li, Max Ruiz Luyten, and Mihaela van der Schaar. Risk-sensitive diffusion: Robustly optimizing diffusion models with noisy samples. In *International Conference on Learning Representations*, 2024.
- Sheng Liu, Jonathan Niles-Weed, Narges Razavian, and Carlos Fernandez-Granda. Early-learning regularization prevents memorization of noisy labels. In *Advances in Neural Information Processing Systems*, pp. 20331–20342, 2020.
- Songhua Liu, Kai Wang, Xingyi Yang, Jingwen Ye, and Xinchao Wang. Dataset distillation via factorization. In *Advances in Neural Information Processing Systems*, pp. 1100–1113, 2022.
- Noel Loo, Ramin Hasani, Alexander Amini, and Daniela Rus. Efficient dataset distillation using random feature approximation. In *Advances in Neural Information Processing Systems*, pp. 13877–13891, 2022.
- Calvin Luo. Understanding diffusion models: A unified perspective. *arXiv preprint arXiv:2208.11970*, 2022.
- Wenshui Luo, Shuo Chen, Tongliang Liu, Bo Han, Gang Niu, Masashi Sugiyama, Dacheng Tao, and Chen Gong. Estimating per-class statistics for label noise learning. *IEEE Transactions on Pattern Analysis and Machine Intelligence*, 47(1):305–322, 2024.
- Jiaqi Lv, Miao Xu, Lei Feng, Gang Niu, Xin Geng, and Masashi Sugiyama. Progressive identification of true labels for partial-label learning. In *Proceedings of the International Conference on Machine Learning*, pp. 6500–6510, 2020.
- Eran Malach and Shai Shalev-Shwartz. Decoupling” when to update” from” how to update”. In *Advances in Neural Information Processing Systems*, pp. 960–970, 2017.
- Takeru Miyato and Masanori Koyama. cgans with projection discriminator. In *International Conference on Learning Representations*, 2018.
- Takeru Miyato, Shin-ichi Maeda, Masanori Koyama, and Shin Ishii. Virtual adversarial training: a regularization method for supervised and semi-supervised learning. *IEEE Transactions on Pattern Analysis and Machine Intelligence*, 41(8):1979–1993, 2018.

- Byeonghu Na, Yeongmin Kim, HeeSun Bae, Jung Hyun Lee, Se Jung Kwon, Wanmo Kang, and Il-Chul Moon. Label-noise robust diffusion models. In *International Conference on Learning Representations*, 2024.
- Muhammad Ferjad Naeem, Seong Joon Oh, Youngjung Uh, Yunjey Choi, and Jaejun Yoo. Reliable fidelity and diversity metrics for generative models. In *Proceedings of the International Conference on Machine Learning*, pp. 7176–7185, 2020.
- Timothy Nguyen, Roman Novak, Lechao Xiao, and Jaehoon Lee. Dataset distillation with infinitely wide convolutional networks. In *Advances in Neural Information Processing Systems*, pp. 5186–5198, 2021.
- Yidong Ouyang, Liyan Xie, Chongxuan Li, and Guang Cheng. Missdiff: Training diffusion models on tabular data with missing values. *arXiv preprint arXiv:2307.00467*, 2023.
- Adam Paszke, Sam Gross, Francisco Massa, Adam Lerer, James Bradbury, Gregory Chanan, Trevor Killeen, Zeming Lin, Natalia Gimelshein, Luca Antiga, et al. Pytorch: An imperative style, high-performance deep learning library. In *Advances in Neural Information Processing Systems*, 2019.
- Congyu Qiao, Ning Xu, and Xin Geng. Decompositional generation process for instance-dependent partial label learning. In *International Conference on Learning Representations*, 2023.
- Antti Rasmus, Mathias Berglund, Mikko Honkala, Harri Valpola, and Tapani Raiko. Semi-supervised learning with ladder networks. In *Advances in Neural Information Processing Systems*, pp. 3546–3554, 2015.
- Robin Rombach, Andreas Blattmann, Dominik Lorenz, Patrick Esser, and Bjorn Ommer. High-resolution image synthesis with latent diffusion models. In *IEEE/CVF Conference on Computer Vision and Pattern Recognition*, pp. 23464–23473, 2022.
- Chitwan Saharia, William Chan, Saurabh Saxena, Lala Li, Jay Whang, Emily L Denton, Kamyar Ghasemipour, Raphael Gontijo Lopes, Burcu Karagol Ayan, Tim Salimans, et al. Photorealistic text-to-image diffusion models with deep language understanding. pp. 36479–36494, 2022.
- Ahmad Sajedi, Samir Khaki, Ehsan Amjadian, Lucy Z. Liu, Yuri A. Lawryshyn, and Konstantinos N. Plataniotis. Datadam: Efficient dataset distillation with attention matching. In *Proceedings of the IEEE/CVF International Conference on Computer Vision*, pp. 17097–17107, 2023.
- Tim Salimans and Jonathan Ho. Progressive distillation for fast sampling of diffusion models. In *International Conference on Learning Representations*, 2022.
- Tim Salimans, Ian Goodfellow, Wojciech Zaremba, Vicki Cheung, Alec Radford, and Xi Chen. Improved techniques for training gans. In *Advances in Neural Information Processing Systems*, pp. 2226–2234, 2016.
- Shitong Shao, Zikai Zhou, Huanran Chen, and Zhiqiang Shen. Elucidating the design space of dataset condensation. In *Advances in Neural Information Processing Systems*, pp. 99161–99201, 2024.
- Donghyeok Shin, Seungjae Shin, and Il-Chul Moon. Frequency domain-based dataset distillation. In *Advances in Neural Information Processing Systems*, pp. 70033–70044, 2024.
- Vinay Shukla, Zhe Zeng, Kareem Ahmed, and Guy Van den Broeck. A unified approach to count-based weakly supervised learning. In *Advances in Neural Information Processing Systems*, pp. 38709–38722, 2023.
- Kihyuk Sohn, David Berthelot, Nicholas Carlini, Zizhao Zhang, Han Zhang, Colin A Raffel, Ekin Dogus Cubuk, Alexey Kurakin, and Chun-Liang Li. Fixmatch: Simplifying semi-supervised learning with consistency and confidence. In *Advances in Neural Information Processing Systems*, pp. 596–608, 2020.
- Yang Song and Stefano Ermon. Generative modeling by estimating gradients of the data distribution. In *Advances in Neural Information Processing Systems*, pp. 11895–11907, 2019.

- Yang Song and Stefano Ermon. Improved techniques for training score-based generative models. In *Advances in Neural Information Processing Systems*, pp. 12438–12448, 2020.
- Yang Song, Jascha Sohl-Dickstein, Diederik P Kingma, Abhishek Kumar, Stefano Ermon, and Ben Poole. Score-based generative modeling through stochastic differential equations. In *International Conference on Learning Representations*, 2020.
- Yang Song, Conor Durkan, Iain Murray, and Stefano Ermon. Maximum likelihood training of score-based diffusion models. In *Advances in Neural Information Processing Systems*, pp. 1415–1428, 2021.
- Peng Sun, Bei Shi, Daiwei Yu, and Tao Lin. On the diversity and realism of distilled dataset: An efficient dataset distillation paradigm. In *IEEE/CVF Conference on Computer Vision and Pattern Recognition*, pp. 9390–9399, 2024.
- Christian Szegedy, Vincent Vanhoucke, Sergey Ioffe, Jon Shlens, and Zbigniew Wojna. Rethinking the inception architecture for computer vision. In *IEEE/CVF Conference on Computer Vision and Pattern Recognition*, pp. 2818–2826, 2016.
- Hiroshi Takahashi, Tomoharu Iwata, Atsutoshi Kumagai, Yuuki Yamanaka, and Tomoya Yamashita. Positive-unlabeled diffusion models for preventing sensitive data generation. In *International Conference on Learning Representations*, 2025.
- Antti Tarvainen and Harri Valpola. Mean teachers are better role models: Weight-averaged consistency targets improve semi-supervised deep learning results. In *Advances in Neural Information Processing Systems*, pp. 1195–1204, 2017.
- Yingjie Tian, Xiaotong Yu, and Saiji Fu. Partial label learning: Taxonomy, analysis and outlook. *Neural Networks*, 161:708–734, 2023.
- Pascal Vincent. A connection between score matching and denoising autoencoders. *Neural computation*, 23(7):1661–1674, 2011.
- Haobo Wang, Mingxuan Xia, Yixuan Li, Yuren Mao, Lei Feng, Gang Chen, and Junbo Zhao. Solar: Sinkhorn label refinery for imbalanced partial-label learning. In *Advances in Neural Information Processing Systems*, pp. 8104–8117, 2022a.
- Haobo Wang, Ruixuan Xiao, Yixuan Li, Lei Feng, Gang Niu, Gang Chen, and Junbo Zhao. Pico+: Contrastive label disambiguation for robust partial label learning. *IEEE Transactions on Pattern Analysis and Machine Intelligence*, pp. 3183–3198, 2023.
- Hsiu-Hsuan Wang, Tan-Ha Mai, Nai-Xuan Ye, Wei-I Lin, and Hsuan-Tien Lin. Climage: Human-annotated datasets for complementary-label learning. *Transactions on Machine Learning Research*, 2025, 2025a.
- Kai Wang, Bo Zhao, Xiangyu Peng, Zheng Zhu, Shuo Yang, Shuo Wang, Guan Huang, Hakan Bilen, Xinchao Wang, and Yang You. Cafe: Learning to condense dataset by aligning features. In *IEEE/CVF Conference on Computer Vision and Pattern Recognition*, pp. 12196–12205, 2022b.
- Tongzhou Wang, Jun-Yan Zhu, Antonio Torralba, and Alexei A Efros. Dataset distillation. *arXiv preprint arXiv:1811.10959*, 2018.
- Wei Wang, Dong-Dong Wu, Jindong Wang, Gang Niu, Min-Ling Zhang, and Masashi Sugiyama. Realistic evaluation of deep partial-label learning algorithms. In *International Conference on Learning Representations*, 2025b.
- Yidong Wang, Hao Chen, Yue Fan, Wang Sun, Ran Tao, Wenxin Hou, Renjie Wang, Linyi Yang, Zhi Zhou, Lan-Zhe Guo, et al. Usb: A unified semi-supervised learning benchmark for classification. In *Advances in Neural Information Processing Systems*, pp. 3938–3961, 2022c.
- Yidong Wang, Hao Chen, Qiang Heng, Wenxin Hou, Yue Fan, Zhen Wu, Jindong Wang, Marios Savvides, Takahiro Shinozaki, Bhiksha Raj, et al. Freematch: Self-adaptive thresholding for semi-supervised learning. In *International Conference on Learning Representations*, 2022d.

- Yisen Wang, Xingjun Ma, Zaiyi Chen, Yuan Luo, Jinfeng Yi, and James Bailey. Symmetric cross entropy for robust learning with noisy labels. In *Proceedings of the IEEE/CVF International Conference on Computer Vision*, pp. 322–330, 2019.
- Hongxin Wei, Lei Feng, Xiangyu Chen, and Bo An. Combating noisy labels by agreement: A joint training method with co-regularization. In *IEEE/CVF Conference on Computer Vision and Pattern Recognition*, pp. 13726–13735, 2020.
- Jiaheng Wei, Zhaowei Zhu, Hao Cheng, Tongliang Liu, Gang Niu, and Yang Liu. Learning with noisy labels revisited: A study using real-world human annotations. In *International Conference on Learning Representations*, 2021.
- Zixi Wei, Lei Feng, Bo Han, Tongliang Liu, Gang Niu, Xiaofeng Zhu, and Heng Tao Shen. A universal unbiased method for classification from aggregate observations. In *Proceedings of the International Conference on Machine Learning*, pp. 36804–36820, 2023.
- Hongwei Wen, Jingyi Cui, Hanyuan Hang, Jiabin Liu, Yisen Wang, and Zhouchen Lin. Leveraged weighted loss for partial label learning. In *Proceedings of the International Conference on Machine Learning*, pp. 11091–11100, 2021.
- Dong-Dong Wu, Deng-Bao Wang, and Min-Ling Zhang. Revisiting consistency regularization for deep partial label learning. In *Proceedings of the International Conference on Machine Learning*, pp. 24212–24225, 2022.
- Dong-Dong Wu, Deng-Bao Wang, and Min-Ling Zhang. Distilling reliable knowledge for instance-dependent partial label learning. In *Proceedings of the AAAI Conference on Artificial Intelligence*, pp. 15888–15896, 2024.
- Shiyu Xia, Jiaqi Lv, Ning Xu, and Xin Geng. Ambiguity-induced contrastive learning for instance-dependent partial label learning. In *Proceedings of the International Joint Conference on Artificial Intelligence*, pp. 3615–3621, 2022.
- Han Xiao, Kashif Rasul, and Roland Vollgraf. Fashion-mnist: a novel image dataset for benchmarking machine learning algorithms. *arXiv preprint arXiv:1708.07747*, 2017.
- Enze Xie, Junsong Chen, Junyu Chen, Han Cai, Haotian Tang, Yujun Lin, Zhekai Zhang, Muyang Li, Ligeng Zhu, Yao Lu, et al. Sana: Efficient high-resolution image synthesis with linear diffusion transformers. In *International Conference on Learning Representations*, 2025.
- Qizhe Xie, Zihang Dai, Eduard Hovy, Thang Luong, and Quoc Le. Unsupervised data augmentation for consistency training. In *Advances in Neural Information Processing Systems*, pp. 6256–6268, 2020.
- Zheng Xie, Yu Liu, Hao-Yuan He, Ming Li, and Zhi-Hua Zhou. Weakly supervised auc optimization: A unified partial auc approach. *IEEE Transactions on Pattern Analysis and Machine Intelligence*, 46(7):4780–4795, 2024.
- Ning Xu, Biao Liu, Jiaqi Lv, Congyu Qiao, and Xin Geng. Progressive purification for instance-dependent partial label learning. In *Proceedings of the International Conference on Machine Learning*, pp. 38551–38565, 2023.
- Yi Xu, Lei Shang, Jinxing Ye, Qi Qian, Yu-Feng Li, Baigui Sun, Hao Li, and Rong Jin. Dash: Semi-supervised learning with dynamic thresholding. In *Proceedings of the International Conference on Machine Learning*, pp. 11525–11536, 2021.
- Eric Xue, Yijiang Li, Haoyang Liu, Peiran Wang, Yifan Shen, and Haohan Wang. Towards adversarially robust dataset distillation by curvature regularization. In *Proceedings of the AAAI Conference on Artificial Intelligence*, pp. 9041–9049, 2025.
- Muqiao Yang, Chunlei Zhang, Yong Xu, Zhongweiyang Xu, Heming Wang, Bhiksha Raj, and Dong Yu. Usee: Unified speech enhancement and editing with conditional diffusion models. In *IEEE International Conference on Acoustics, Speech and Signal Processing*, pp. 7125–7129, 2024.

- Xiangli Yang, Zixing Song, Irwin King, and Zenglin Xu. A survey on deep semi-supervised learning. *IEEE transactions on knowledge and data engineering*, 35(9):8934–8954, 2022.
- Yu Yao, Tongliang Liu, Bo Han, Mingming Gong, Jiankang Deng, Gang Niu, and Masashi Sugiyama. Dual t: Reducing estimation error for transition matrix in label-noise learning. pp. 7260–7271, 2020.
- Kun Yi and Jianxin Wu. Probabilistic end-to-end noise correction for learning with noisy labels. In *IEEE/CVF Conference on Computer Vision and Pattern Recognition*, pp. 7017–7025, 2019.
- Zeyuan Yin and Zhiqiang Shen. Dataset distillation via curriculum data synthesis in large data era. *Transactions on Machine Learning Research*, 2024.
- Zeyuan Yin, Eric Xing, and Zhiqiang Shen. Squeeze, recover and relabel: Dataset condensation at imagenet scale from a new perspective. In *Advances in Neural Information Processing Systems*, pp. 73582–73603, 2024.
- Xingrui Yu, Bo Han, Jiangchao Yao, Gang Niu, Ivor Tsang, and Masashi Sugiyama. How does disagreement help generalization against label corruption? In *Proceedings of the International Conference on Machine Learning*, pp. 7164–7173, 2019.
- Bowen Zhang, Yidong Wang, Wenxin Hou, Hao Wu, Jindong Wang, Manabu Okumura, and Takahiro Shinozaki. Flexmatch: Boosting semi-supervised learning with curriculum pseudo labeling. In *Advances in Neural Information Processing Systems*, pp. 18408–18419, 2021a.
- Fei Zhang, Lei Feng, Bo Han, Tongliang Liu, Gang Niu, Tao Qin, and Masashi Sugiyama. Exploiting class activation value for partial-label learning. In *International Conference on Learning Representations*, 2021b.
- Hongyi Zhang, Moustapha Cisse, Yann N Dauphin, and David Lopez-Paz. mixup: Beyond empirical risk minimization. In *International Conference on Learning Representations*, 2018.
- Yivan Zhang, Nontawat Charoenphakdee, Zhenguo Wu, and Masashi Sugiyama. Learning from aggregate observations. In *Advances in Neural Information Processing Systems*, pp. 7993–8005, 2020.
- Zhilu Zhang and Mert Sabuncu. Generalized cross entropy loss for training deep neural networks with noisy labels. In *Advances in Neural Information Processing Systems*, pp. 8792–8802, 2018.
- Bo Zhao and Hakan Bilen. Dataset condensation with differentiable siamese augmentation. In *Proceedings of the International Conference on Machine Learning*, pp. 12674–12685, 2021.
- Bo Zhao and Hakan Bilen. Dataset condensation with distribution matching. In *Proceedings of the IEEE/CVF winter conference on applications of computer vision*, pp. 6514–6523, 2023.
- Bo Zhao, Konda Reddy Mopuri, and Hakan Bilen. Dataset condensation with gradient matching. In *International Conference on Learning Representations*, 2021.
- Chen Zhao, Weiling Cai, Chenyu Dong, and Chengwei Hu. Wavelet-based fourier information interaction with frequency diffusion adjustment for underwater image restoration. In *IEEE/CVF Conference on Computer Vision and Pattern Recognition*, pp. 8281–8291, 2024.
- Mingkai Zheng, Shan You, Lang Huang, Fei Wang, Chen Qian, and Chang Xu. Simmatch: Semi-supervised learning with similarity matching. In *IEEE/CVF Conference on Computer Vision and Pattern Recognition*, pp. 14471–14481, 2022.
- Yongchao Zhou, Ehsan Nezhadarya, and Jimmy Ba. Dataset distillation using neural feature regression. In *Advances in Neural Information Processing Systems*, pp. 9813–9827, 2022.

## CONTENTS

<b>1</b>	<b>Introduction</b>	<b>1</b>
<b>2</b>	<b>Background</b>	<b>2</b>
<b>3</b>	<b>Methodology</b>	<b>3</b>
3.1	Unified Learning Objective . . . . .	3
3.2	Generative Objective: Modeling the Imprecise Data Distribution . . . . .	3
3.3	Classification Objective: Inferring Labels from Imprecise Signals . . . . .	4
<b>4</b>	<b>Time Complexity Reduction</b>	<b>5</b>
<b>5</b>	<b>Experiments</b>	<b>7</b>
5.1	Task1: Image Generation . . . . .	8
5.2	Task2: Weakly Supervised Learning . . . . .	8
5.3	Task3: Noisy Dataset Condensation . . . . .	9
<b>6</b>	<b>Conclusion</b>	<b>9</b>
<b>A</b>	<b>Notation and Definitions</b>	<b>19</b>
<b>B</b>	<b>Proof</b>	<b>19</b>
B.1	Connections among Different Diffusion Models. . . . .	19
B.2	Derivation of Eq. (5) . . . . .	20
B.3	Derivation of Variational Lower Bound Eq. (7) . . . . .	22
B.4	Derivation of Conditional ELBO in Eq. (8). . . . .	23
B.5	Derivation of Remark 1 . . . . .	23
B.6	Proof of Theorem 1 . . . . .	25
B.7	Proof of Proposition 1 . . . . .	26
B.8	Proof of Theorem 2 . . . . .	26
B.9	Proof of Theorem 3 . . . . .	27
<b>C</b>	<b>Discussion</b>	<b>28</b>
C.1	Analysis of Early-Learning Regularization in Eq. (15) . . . . .	28
C.2	Class-Prior Estimation in Imprecise-Label Datasets . . . . .	29
<b>D</b>	<b>Implementation Details</b>	<b>30</b>
<b>E</b>	<b>Experiments</b>	<b>31</b>
E.1	Evaluation Metrics . . . . .	31
E.2	Full Results in Weakly Supervised Learning . . . . .	31
E.3	Integration with Existing Imprecise-Label Correctors . . . . .	33

E.4	Comparison of Accuracy Curves between <i>DMIS</i> and <i>Vanilla</i> . . . . .	33
E.5	Visualization of Noisy Condensed Datasets . . . . .	33
E.6	Additional Results on Dataset Condensation under Different Forms of Imprecise Supervision . . . . .	34
<b>F</b>	<b>Related Work</b>	<b>35</b>
F.1	Robust Diffusion Models . . . . .	35
F.2	Imprecise Label Learning . . . . .	35
F.3	Dataset Condensation . . . . .	35

**The Use of Large Language Models (LLMs).** LLMs were only used for language polishing and proofreading. No part of the technical content, experiments, or analysis was generated by LLMs.

## A NOTATION AND DEFINITIONS

We present the notation table for each symbol used in this paper in Table 4.

Table 4: List of common mathematical symbols used in this paper.

Symbol	Definition
$\mathbf{x}$	A sample of training data
$z$	Imprecise label associated with a sample
$s$	Candidate label set for a sample
$y$	Class index label
$c$	Total number of classes
$\mathcal{X}$	Input space from which $\mathbf{x}$ is drawn
$\mathcal{Y}$	Label space from which $y$ is drawn
$X$	Random variable for training instances
$Y$	Random variable for true labels
$Z$	Random variable for imprecise labels
$S$	Random variable for partial labels
$\hat{Y}$	Random variable for noisy labels
$X^l$	Set of labeled data instances
$X^u$	Set of unlabeled data instances
$Y^l$	Set of labels corresponding to $X^l$
$\emptyset$	Empty label set
$\theta$	Parameters of the diffusion model to be optimized
$\phi$	Exponential moving average of $\theta$ over training iteration
$\mathbf{0}$	Zero vector
$\mathbf{I}$	Identity matrix
$\mathbf{x}_t$	Noisy version of the sample at timestep $t$
$\tau$	Continuous timestep variable
$\alpha_t$	Scaling factor at timestep $t$
$\sigma_t$	Noise scale at timestep $t$
$l$	Left boundary of a subsampled timestep interval
$r$	Right boundary of a subsampled timestep interval
$\Delta$	Length of a subsampled timestep interval
$q(\cdot)$	Real Data distribution
$q(\cdot   \cdot)$	Real conditional data distribution
$p(\cdot)$	Marginal probability distribution
$p(\cdot   \cdot)$	Model-inferred conditional distribution
$F(\cdot)$	Cumulative distribution function of $p(\cdot)$
$f(\cdot)$	Diffusion classifier
$\mathbf{s}(\cdot, \cdot)$	Time-conditioned score prediction network
$\mathcal{N}(\cdot, \cdot)$	Gaussian distribution

## B PROOF

### B.1 CONNECTIONS AMONG DIFFERENT DIFFUSION MODELS.

The diffusion model we define in this paper can be reformulated to align with other common diffusion frameworks, such as DDPM (Ho et al., 2020), SMLD (Song & Ermon, 2019), VE-SDE (Song et al., 2020) and VP-SDE (Song et al., 2020), as well as with approaches like x-prediction (Ho et al., 2020), v-prediction (Salimans & Ho, 2022), and  $\epsilon$ -prediction (Ho et al., 2020). This demonstrates that our formulation is compatible with diverse diffusion paradigms while facilitating unified theoretical analysis. To better demonstrate this transformation, we present the following pseudocodes.

**Algorithm 1** Our models to EDM

---

**Require:** A score network  $s_\theta$ , a noisy input  $\mathbf{x}_t$ , noise level  $t$ , linear schedule  $\{\alpha_i\}_{i=1}^T$  and  $\{\sigma_i\}_{i=1}^T$ .

- 1: Calculate the denoised image  $\mathbf{x}_0$  using  $s_\theta$ :  $\mathbf{x}_0 = (\mathbf{x}_t + \sigma_t^2 s_\theta(\mathbf{x}_t/\alpha_t, \sigma_t/\alpha_t))/\alpha_t$
- 2: **if** performing  $\mathbf{x}_0$ -prediction **then**
- 3:     **return**  $\mathbf{x}_0$ .
- 4: **end if**
- 5: Calculate the noise component  $\epsilon$ :  $\epsilon = \frac{\mathbf{x}_t - \alpha_t \mathbf{x}_0}{\sigma_t}$
- 6: **if** performing  $\epsilon$ -prediction **then**
- 7:     **return**  $\epsilon$ .
- 8: **end if**
- 9: Calculate the noise component  $\mathbf{v}$ :  $\mathbf{v} = \alpha_t \epsilon - \sigma_t \mathbf{x}_0$
- 10: **if** performing  $\mathbf{v}$ -prediction **then**
- 11:     **return**  $\mathbf{v}$ .
- 12: **end if**

---

**DDPM.** DDPM define a sequence  $\{\beta_t\}_{t=0}^T$  and  $\mathbf{x}_t = \sqrt{\prod_{i=0}^t (1 - \beta_i)} \mathbf{x}_0 + \sqrt{1 - \prod_{i=0}^t (1 - \beta_i)} \epsilon$ , which can be seen as a special case of Eq. (1) where we can set  $\alpha_t = \sqrt{\prod_{i=0}^t (1 - \beta_i)}$  and  $\sigma_t = \sqrt{1 - \prod_{i=0}^t (1 - \beta_i)}$ .

**SMLD.** SMLD defines a noise schedule  $\sigma(t)_{t=0}^T$  and  $\mathbf{x}_t = \mathbf{x}_0 + \sigma(t)\epsilon$ , with  $\sigma(1) < \sigma(2) < \dots < \sigma(T)$ . In this setup, Eq. (1) reduces to  $\alpha_t = 1, \sigma_t = \sigma(t)$ .

**VP-SDE.** VP-SDE is the continuous case of DDPM, which define a stochastic differential equation (SDE) as

$$dX_t = -\frac{1}{2}\beta(t)X_t dt + \sqrt{\beta(t)}dW_t, \quad t \in [0, 1],$$

where  $\beta(t) = \beta_{t,T} \cdot T$ . In this setup,  $\alpha_t = \sqrt{\exp\left(-\int_0^t \beta(s)ds\right)}$ ,  $\sigma_t = 1 - \exp\left(-\int_0^t \beta(s)ds\right)$ .

**VE-SDE.** VE-SDE is the continuous case of SMLD, whose forward process of VE-SDE is defined as

$$dX_t = \sqrt{\frac{d\sigma(t)^2}{dt}} dW_t.$$

In this setup,  $\alpha_t = 1$  and  $\sigma_t = \sqrt{\sigma^2(t) - \sigma^2(0)}$ .

While the models above each define their own specific frameworks for the diffusion process, EDM (Karras et al., 2022) proposes a unified structure and optimizes the parameters choice within the diffusion process, making it both robust and adaptable. Therefore, for our implementation, we adopt EDM as the foundational diffusion model. In EDM, the scaling and noise schedules are a special case of VE-SDE, where the variance of the noise is given by  $\sigma(t) = t$ . Accordingly, we use  $s_\theta(\mathbf{x}/\alpha_t, \sigma_t/\alpha_t)$  to obtain the predicted score, as shown in Algorithm 1.

## B.2 DERIVATION OF EQ. (5)

Maximizing the variational lower bound, or equivalently evidence lower bound (ELBO), to optimize the diffusion model is a common approach. To avoid redundant proofs, we directly use the conclusion from Eq. (58) in Luo (2022) as below:

$$\log p_\theta(\mathbf{x}) \geq \mathbb{E}_q[-D_{\text{KL}}(q(\mathbf{x}_T|\mathbf{x}_0)||p(\mathbf{x}_T)) + \log p_\theta(\mathbf{x}_0|\mathbf{x}_1) - \sum_{t>1} D_{\text{KL}}(q(\mathbf{x}_{t-1}|\mathbf{x}_t, \mathbf{x}_0)||p_\theta(\mathbf{x}_{t-1}|\mathbf{x}_t))]$$

Although each KL divergence term  $D_{\text{KL}}(q(\mathbf{x}_{t-1}|\mathbf{x}_t, \mathbf{x}_0)||p_\theta(\mathbf{x}_{t-1}|\mathbf{x}_t))$  is difficult to minimize for arbitrary posteriors, we can leverage the Gaussian transition assumption to make optimization tractable. By Bayes rule, we have:

$$q(\mathbf{x}_{t-1}|\mathbf{x}_t, \mathbf{x}_0) = \frac{q(\mathbf{x}_t|\mathbf{x}_{t-1}, \mathbf{x}_0)q(\mathbf{x}_{t-1}|\mathbf{x}_0)}{q(\mathbf{x}_t|\mathbf{x}_0)}$$

As we already know that  $q(\mathbf{x}_t|\mathbf{x}_0)$  and  $q(\mathbf{x}_{t-1}|\mathbf{x}_0)$  from Eq. (1),  $q(\mathbf{x}_t|\mathbf{x}_{t-1}, \mathbf{x}_0)$  can be derived from its equivalent form  $q(\mathbf{x}_t|\mathbf{x}_{t-1})$  as follows:

$$\begin{aligned}
\mathbf{x}_t &= \alpha_t \mathbf{x}_0 + \sigma_t \boldsymbol{\epsilon}_0 \\
&= \alpha_t \left( \frac{\mathbf{x}_{t-1} - \sigma_{t-1} \boldsymbol{\epsilon}_0^*}{\alpha_{t-1}} \right) + \sigma_t \boldsymbol{\epsilon}_0 \\
&= \frac{\alpha_t}{\alpha_{t-1}} \mathbf{x}_{t-1} + \sigma_t \boldsymbol{\epsilon}_0 - \frac{\alpha_t}{\alpha_{t-1}} \sigma_{t-1} \boldsymbol{\epsilon}_0^* \\
&= \frac{\alpha_t}{\alpha_{t-1}} \mathbf{x}_{t-1} + \sqrt{\sigma_t^2 - \frac{\alpha_t^2}{\alpha_{t-1}^2} \sigma_{t-1}^2} \boldsymbol{\epsilon}_{t-1} \\
&= \mathcal{N}(\mathbf{x}_t; \frac{\alpha_t}{\alpha_{t-1}} \mathbf{x}_{t-1}, \sigma_t^2 - \frac{\alpha_t^2}{\alpha_{t-1}^2} \sigma_{t-1}^2 \mathbf{I}).
\end{aligned}$$

Now, knowing the forms of  $q(\mathbf{x}_t|\mathbf{x}_{t-1}, \mathbf{x}_0)$ , we can proceed to calculate the form of  $q(\mathbf{x}_{t-1}|\mathbf{x}_t, \mathbf{x}_0)$  by substituting into the Bayes rule expansion:

$$\begin{aligned}
q(\mathbf{x}_{t-1}|\mathbf{x}_t, \mathbf{x}_0) &= \frac{q(\mathbf{x}_t|\mathbf{x}_{t-1}, \mathbf{x}_0)q(\mathbf{x}_{t-1}|\mathbf{x}_0)}{q(\mathbf{x}_t|\mathbf{x}_0)} \\
&= \frac{\mathcal{N}(\mathbf{x}_t; \frac{\alpha_t}{\alpha_{t-1}} \mathbf{x}_{t-1}, \sqrt{\sigma_t^2 - \frac{\alpha_t^2}{\alpha_{t-1}^2} \sigma_{t-1}^2} \mathbf{I}) \mathcal{N}(\mathbf{x}_{t-1}; \alpha_{t-1} \mathbf{x}_0, \sigma_{t-1} \mathbf{I})}{\mathcal{N}(\mathbf{x}_t; \alpha_t \mathbf{x}_0, \sigma_t \mathbf{I})} \\
&\propto \exp \left\{ - \left[ \frac{(\mathbf{x}_t - \frac{\alpha_t}{\alpha_{t-1}} \mathbf{x}_{t-1})^2}{2(\sigma_t^2 - \frac{\alpha_t^2}{\alpha_{t-1}^2} \sigma_{t-1}^2)} + \frac{(\mathbf{x}_{t-1} - \alpha_{t-1} \mathbf{x}_0)^2}{2\sigma_{t-1}^2} - \frac{(\mathbf{x}_t - \alpha_t \mathbf{x}_0)^2}{2\sigma_t^2} \right] \right\} \\
&= \exp \left\{ - \frac{1}{2} \left[ \frac{-2\frac{\alpha_t}{\alpha_{t-1}} \mathbf{x}_t \mathbf{x}_{t-1} + (\frac{\alpha_t}{\alpha_{t-1}})^2 \mathbf{x}_{t-1}^2}{\sigma_t^2 - \frac{\alpha_t^2}{\alpha_{t-1}^2} \sigma_{t-1}^2} + \frac{\mathbf{x}_{t-1}^2 - 2\alpha_{t-1} \mathbf{x}_{t-1} \mathbf{x}_0}{\sigma_{t-1}^2} + C(\mathbf{x}_t, \mathbf{x}_0) \right] \right\} \\
&\propto \exp \left\{ - \frac{1}{2} \left[ \left( \frac{(\frac{\alpha_t}{\alpha_{t-1}})^2}{\sigma_t^2 - \frac{\alpha_t^2}{\alpha_{t-1}^2} \sigma_{t-1}^2} + \frac{1}{\sigma_{t-1}^2} \right) \mathbf{x}_{t-1}^2 - 2 \left( \frac{\frac{\alpha_t}{\alpha_{t-1}} \mathbf{x}_t}{\sigma_t^2 - \frac{\alpha_t^2}{\alpha_{t-1}^2} \sigma_{t-1}^2} + \frac{\alpha_{t-1} \mathbf{x}_0}{\sigma_{t-1}^2} \right) \mathbf{x}_{t-1} \right] \right\} \\
&= \exp \left\{ - \frac{1}{2} \left[ \frac{\sigma_{t-1}^2 (\frac{\alpha_t}{\alpha_{t-1}})^2 + (\sigma_t^2 - \frac{\alpha_t^2}{\alpha_{t-1}^2} \sigma_{t-1}^2)}{(\sigma_t^2 - \frac{\alpha_t^2}{\alpha_{t-1}^2} \sigma_{t-1}^2) \sigma_{t-1}^2} \mathbf{x}_{t-1}^2 - 2 \left( \frac{\frac{\alpha_t}{\alpha_{t-1}} \mathbf{x}_t}{\sigma_t^2 - \frac{\alpha_t^2}{\alpha_{t-1}^2} \sigma_{t-1}^2} + \frac{\alpha_{t-1} \mathbf{x}_0}{\sigma_{t-1}^2} \right) \mathbf{x}_{t-1} \right] \right\} \\
&= \exp \left\{ - \frac{1}{2} \left[ \frac{\sigma_t^2}{(\sigma_t^2 - \frac{\alpha_t^2}{\alpha_{t-1}^2} \sigma_{t-1}^2) \sigma_{t-1}^2} \mathbf{x}_{t-1}^2 - 2 \left( \frac{\frac{\alpha_t}{\alpha_{t-1}} \mathbf{x}_t}{\sigma_t^2 - \frac{\alpha_t^2}{\alpha_{t-1}^2} \sigma_{t-1}^2} + \frac{\alpha_{t-1} \mathbf{x}_0}{\sigma_{t-1}^2} \right) \mathbf{x}_{t-1} \right] \right\} \\
&= \exp \left\{ - \frac{1}{2} \left( \frac{\sigma_t^2}{(\sigma_t^2 - \frac{\alpha_t^2}{\alpha_{t-1}^2} \sigma_{t-1}^2) \sigma_{t-1}^2} \right) \left[ \mathbf{x}_{t-1}^2 - 2 \left( \frac{\frac{\frac{\alpha_t}{\alpha_{t-1}} \mathbf{x}_t}{\sigma_t^2 - \frac{\alpha_t^2}{\alpha_{t-1}^2} \sigma_{t-1}^2} + \frac{\alpha_{t-1} \mathbf{x}_0}{\sigma_{t-1}^2}}{\frac{\sigma_t^2}{(\sigma_t^2 - \frac{\alpha_t^2}{\alpha_{t-1}^2} \sigma_{t-1}^2) \sigma_{t-1}^2}} \right) \mathbf{x}_{t-1} \right] \right\} \\
&= \exp \left\{ - \frac{1}{2} \left( \frac{1}{(\sigma_t^2 - \frac{\alpha_t^2}{\alpha_{t-1}^2} \sigma_{t-1}^2) \sigma_{t-1}^2} \right) \left[ \mathbf{x}_{t-1}^2 - 2 \left( \frac{\frac{\alpha_t}{\alpha_{t-1}} \mathbf{x}_t \sigma_{t-1}^2 + (\sigma_t^2 - \frac{\alpha_t^2}{\alpha_{t-1}^2} \sigma_{t-1}^2) \alpha_{t-1} \mathbf{x}_0}{\sigma_t^2} \right) \mathbf{x}_{t-1} \right] \right\} \\
&\propto \mathcal{N}(\mathbf{x}_{t-1}; \frac{\frac{\alpha_t}{\alpha_{t-1}} \mathbf{x}_t \sigma_{t-1}^2 + (\sigma_t^2 - \frac{\alpha_t^2}{\alpha_{t-1}^2} \sigma_{t-1}^2) \alpha_{t-1} \mathbf{x}_0}{\sigma_t^2}, \frac{(\sigma_t^2 - \frac{\alpha_t^2}{\alpha_{t-1}^2} \sigma_{t-1}^2) \sigma_{t-1}^2}{\sigma_t^2} \mathbf{I})
\end{aligned}$$

where in the fourth Equation,  $C(\mathbf{x}_t, \mathbf{x}_0)$  is a constant term with respect to  $\mathbf{x}_{t-1}$  computed as a combination of only  $\mathbf{x}_t$ ,  $\mathbf{x}_0$ , and  $\alpha$  values. We have therefore shown that at each step,  $\mathbf{x}_{t-1} \sim$

$q(\mathbf{x}_{t-1}|\mathbf{x}_t, \mathbf{x}_0)$  is normally distributed, with mean  $\boldsymbol{\mu}_q(\mathbf{x}_t, \mathbf{x}_0)$  that is a function of  $\mathbf{x}_t$  and  $\mathbf{x}_0$ , and variance  $\Sigma_q(t)$  as a function of  $\alpha$  and  $\sigma$  coefficients. These coefficients are known and fixed at each timestep; they are either set permanently when modeled as hyperparameters, or treated as the current inference output of a network that seeks to model them.

We can then set the variances of the two Gaussians to match exactly, optimizing the KL Divergence term reduces to minimizing the difference between the means of the two distributions:

$$\begin{aligned} & \arg \min_{\theta} D_{\text{KL}}(q(\mathbf{x}_{t-1}|\mathbf{x}_t, \mathbf{x}_0) \| p_{\theta}(\mathbf{x}_{t-1}|\mathbf{x}_t)) \\ &= \arg \min_{\theta} \frac{1}{2\sigma_q^2(t)} \left[ \|\boldsymbol{\mu}_{\theta}(\mathbf{x}_t, t) - \boldsymbol{\mu}_q(\mathbf{x}_t, \mathbf{x}_0)\|_2^2 \right], \end{aligned} \quad (18)$$

where  $\sigma_q^2(t) = \frac{(\sigma_t^2 - \frac{\alpha_t^2}{\alpha_{t-1}^2} \sigma_{t-1}^2) \sigma_{t-1}^2}{\sigma_t^2}$ , the derivation is the same as in Eq. (92) in Luo (2022), so we skip the derivation here. To derive the score matching function, we appeal to Tweedie's Formula Efron (2011), which states  $\mathbb{E}[\boldsymbol{\mu}_z|z] = z + \Sigma_z \nabla_z \log q(z)$  for a given Gaussian variable  $z \sim \mathcal{N}(z; \boldsymbol{\mu}_z, \Sigma_z)$ . In this case, we apply it to predict the true posterior mean of  $\mathbf{x}_t$  given its samples. We can obtain:

$$\begin{aligned} \mathbb{E}[\boldsymbol{\mu}_{\mathbf{x}_t}|\mathbf{x}_t] &= \mathbf{x}_t + \sigma_t^2 \nabla_{\mathbf{x}_t} \log q(\mathbf{x}_t) = \alpha_t \mathbf{x}_0 \\ \therefore \mathbf{x}_0 &= \frac{\mathbf{x}_t + \sigma_t^2 \nabla_{\mathbf{x}_t} \log q(\mathbf{x}_t)}{\alpha_t} \end{aligned} \quad (19)$$

Then, we can plug Eq. (19) into our ground-truth denoising transition mean  $\boldsymbol{\mu}_q(\mathbf{x}_t, \mathbf{x}_0)$  once again and derive a new form:

$$\begin{aligned} \boldsymbol{\mu}_q(\mathbf{x}_t, \mathbf{x}_0) &= \frac{\frac{\alpha_t}{\alpha_{t-1}} \sigma_{t-1}^2 \mathbf{x}_t + (\sigma_t^2 - \frac{\alpha_t^2}{\alpha_{t-1}^2} \sigma_{t-1}^2) \alpha_{t-1} \cdot \frac{\mathbf{x}_t + \sigma_t^2 \nabla_{\mathbf{x}_t} \log q(\mathbf{x}_t)}{\alpha_t}}{\sigma_t^2} \\ &= \frac{\frac{\alpha_t}{\alpha_{t-1}} \sigma_{t-1}^2}{\sigma_t^2} \mathbf{x}_t + \frac{\sigma_t^2 - \frac{\alpha_t^2}{\alpha_{t-1}^2} \sigma_{t-1}^2}{\sigma_t^2 \frac{\alpha_t}{\alpha_{t-1}}} \mathbf{x}_t + \frac{(\sigma_t^2 - \frac{\alpha_t^2}{\alpha_{t-1}^2} \sigma_{t-1}^2) \sigma_t^2 \nabla_{\mathbf{x}_t} \log q(\mathbf{x}_t)}{\sigma_t^2 \frac{\alpha_t}{\alpha_{t-1}}} \\ &= \frac{\alpha_{t-1}}{\alpha_t} \mathbf{x}_t + \left( \frac{\alpha_{t-1}}{\alpha_t} \sigma_t^2 - \frac{\alpha_t}{\alpha_{t-1}} \sigma_{t-1}^2 \right) \nabla_{\mathbf{x}_t} \log q(\mathbf{x}_t) \\ &= \frac{\alpha_{t-1}}{\alpha_t} \left[ \mathbf{x}_t + \left( \sigma_t^2 - \frac{\alpha_t^2}{\alpha_{t-1}^2} \sigma_{t-1}^2 \right) \mathbf{s}_{\theta}(\mathbf{x}_t, t) \right] \end{aligned} \quad (20)$$

Finally, we plug Eq. (20) into our optimization function Eq. (18), and we can get:

$$\begin{aligned} & \arg \min_{\theta} D_{\text{KL}}(q(\mathbf{x}_{t-1}|\mathbf{x}_t, \mathbf{x}_0) \| p_{\theta}(\mathbf{x}_{t-1}|\mathbf{x}_t)) \\ &= \arg \min_{\theta} \frac{1}{2\sigma_q^2(t)} \left[ \|\boldsymbol{\mu}_{\theta}(\mathbf{x}_t, t) - \boldsymbol{\mu}_q(\mathbf{x}_t, \mathbf{x}_0)\|_2^2 \right] \\ &= \arg \min_{\theta} \frac{1}{2 \frac{(\sigma_t^2 - \frac{\alpha_t^2}{\alpha_{t-1}^2} \sigma_{t-1}^2) \sigma_{t-1}^2}{\sigma_t^2}} \cdot \left( \frac{\alpha_{t-1}}{\alpha_t} \right)^2 \cdot (\sigma_t^2 - \frac{\alpha_t^2}{\alpha_{t-1}^2} \sigma_{t-1}^2)^2 \|\mathbf{s}_{\theta}(\mathbf{x}_t, t) - \nabla_{\mathbf{x}_t} \log q(\mathbf{x}_t)\|_2^2 \\ &= \frac{\sigma_t^2}{2} \left( \frac{\sigma_t^2 \alpha_{t-1}^2}{\sigma_{t-1}^2 \alpha_t^2} - 1 \right) \|\mathbf{s}_{\theta}(\mathbf{x}_t, t) - \nabla_{\mathbf{x}_t} \log q(\mathbf{x}_t)\|_2^2 \end{aligned}$$

### B.3 DERIVATION OF VARIATIONAL LOWER BOUND EQ. (7)

To model  $\log p_{\theta}(X, Z)$ , we introduce an auxiliary distribution  $Q(Y)$  over the latent variable  $Y$ :

$$\begin{aligned} \log p_{\theta}(X, Z) &= \int Q(Y) \log p_{\theta}(X, Z) dY \\ &= \int Q(Y) \log p_{\theta}(X, Z) \frac{p_{\theta}(Y|X, Z)}{p_{\theta}(Y|X, Z)} dY \\ &= \int Q(Y) \log \frac{p_{\theta}(X, Y, Z)}{Q(Y)} dY - \int Q(Y) \log \frac{p_{\theta}(Y|X, Z)}{Q(Y)} dY, \end{aligned}$$

where the first term is the ELBO and the second term is the KL divergence  $\mathcal{D}_{\text{KL}}(Q(Y)||p_\theta(Y|X, Z))$ . Since the KL divergence is non-negative, maximizing the ELBO provides a valid surrogate for maximizing  $\log p_\theta(X, Z)$ . Replacing  $Q(Y)$  with  $p_\phi(Y|X, Z)$  at each iteration will obtain as follows:

$$\begin{aligned}\theta^* &= \arg \max_{\theta} \log p_\theta(X, Z) \\ &= \arg \max_{\theta} \mathbb{E}_{p_\phi(Y|X, Z)}[\log p_\theta(X, Y, Z)] \\ &= \arg \max_{\theta} \mathbb{E}_{p_\phi(Y|X, Z)}[\log p_\theta(X|Z) + \log p_\theta(Y|X, Z) + \log p_\theta(Z)] \\ &= \arg \max_{\theta} \mathbb{E}_{p_\phi(Y|X, Z)}[\log p_\theta(X|Z)] + \mathbb{E}_{p_\phi(Y|X, Z)}[\log p_\theta(Y|X, Z)] \\ &= \arg \max_{\theta} \log p_\theta(X|Z) + \mathbb{E}_{p_\phi(Y|X, Z)}[\log p_\theta(Y|X, Z)].\end{aligned}$$

which is exactly the variational lower bound presented in Eq. (7).

#### B.4 DERIVATION OF CONDITIONAL ELBO IN EQ. (8)

We provide a derivation of conditional ELBO in the following, which is similar to the unconditional ELBO in Ho et al. (2020).

$$\begin{aligned}& \log p_\theta(\mathbf{x}_0 | z) \\ &= \log \int \frac{p_\theta(\mathbf{x}_{0:T} | z) q(\mathbf{x}_{1:T} | \mathbf{x}_0, z)}{q(\mathbf{x}_{1:T} | \mathbf{x}_0, z)} d\mathbf{x}_{1:T} \\ &= \log \mathbb{E}_{q(\mathbf{x}_{1:T} | \mathbf{x}_0, z)} \left[ \frac{p_\theta(\mathbf{x}_T | z) p_\theta(\mathbf{x}_{0:T-1} | \mathbf{x}_T, z)}{q(\mathbf{x}_{1:T} | \mathbf{x}_0, z)} \right] \\ &\geq \mathbb{E}_{q(\mathbf{x}_{1:T} | \mathbf{x}_0, z)} \left[ \log \frac{p_\theta(\mathbf{x}_T | z) p_\theta(\mathbf{x}_{0:T-1} | \mathbf{x}_T, z)}{q(\mathbf{x}_{1:T} | \mathbf{x}_0, z)} \right] \\ &= \mathbb{E}_{q(\mathbf{x}_{1:T} | \mathbf{x}_0, z)} \left[ \log \frac{p_\theta(\mathbf{x}_T | z) \prod_{i=0}^{T-1} p_\theta(\mathbf{x}_i | \mathbf{x}_{i+1}, z)}{\prod_{i=0}^{T-1} q(\mathbf{x}_{i+1} | \mathbf{x}_i, \mathbf{x}_0, z)} \right] \\ &= \mathbb{E}_{q(\mathbf{x}_{1:T} | \mathbf{x}_0, z)} \left[ \log \frac{p_\theta(\mathbf{x}_T | z) \prod_{i=0}^{T-1} p_\theta(\mathbf{x}_i | \mathbf{x}_{i+1}, z)}{\prod_{i=0}^{T-1} \frac{q(\mathbf{x}_{i+1} | \mathbf{x}_0, z) q(\mathbf{x}_i | \mathbf{x}_{i+1}, \mathbf{x}_0, z)}{q(\mathbf{x}_i | \mathbf{x}_0, z)}} \right] \\ &= \mathbb{E}_{q(\mathbf{x}_{1:T} | \mathbf{x}_0, z)} \left[ \log \frac{p_\theta(\mathbf{x}_T | z) \prod_{i=0}^{T-1} p_\theta(\mathbf{x}_i | \mathbf{x}_{i+1}, z)}{\prod_{i=0}^{T-1} q(\mathbf{x}_i | \mathbf{x}_{i+1}, \mathbf{x}_0, z)} - \log q(\mathbf{x}_T | \mathbf{x}_0, z) \right] \\ &= \mathbb{E}_{q(\mathbf{x}_{1:T} | \mathbf{x}_0, z)} \left[ \log \frac{\prod_{i=0}^{T-1} p_\theta(\mathbf{x}_i | \mathbf{x}_{i+1}, z)}{\prod_{i=0}^{T-1} q(\mathbf{x}_i | \mathbf{x}_{i+1}, \mathbf{x}_0, z)} - \log \frac{q(\mathbf{x}_T | \mathbf{x}_0, z)}{p_\theta(\mathbf{x}_T | z)} \right] \\ &= \sum_{i=0}^{T-1} \mathbb{E}_{q(\mathbf{x}_i, \mathbf{x}_{i+1} | \mathbf{x}_0, z)} \left[ \log \frac{p_\theta(\mathbf{x}_i | \mathbf{x}_{i+1}, z)}{q(\mathbf{x}_i | \mathbf{x}_{i+1}, \mathbf{x}_0, z)} \right] - D_{\text{KL}}(q(\mathbf{x}_T | \mathbf{x}_0, z) || p_\theta(\mathbf{x}_T | z)) \\ &= \sum_{i=0}^{T-1} \mathbb{E}_{q(\mathbf{x}_{i+1} | \mathbf{x}_0, z)} \mathbb{E}_{q(\mathbf{x}_i | \mathbf{x}_{i+1}, \mathbf{x}_0, z)} \left[ \log \frac{p_\theta(\mathbf{x}_i | \mathbf{x}_{i+1}, z)}{q(\mathbf{x}_i | \mathbf{x}_{i+1}, \mathbf{x}_0, z)} \right] - D_{\text{KL}}(q(\mathbf{x}_T | \mathbf{x}_0, z) || p_\theta(\mathbf{x}_T | z)) \\ &= C_3 - \sum_{i=1}^{T-1} \mathbb{E}_{q(\mathbf{x}_{i+1} | \mathbf{x}_0, z)} [D_{\text{KL}}(q(\mathbf{x}_i | \mathbf{x}_{i+1}, \mathbf{x}_0, z) || p_\theta(\mathbf{x}_i | \mathbf{x}_{i+1}, z))] \\ &= -\mathbb{E}_t \left[ w_t \|\mathbf{s}_\theta(\mathbf{x}_t, z, t) - \nabla \log q(\mathbf{x}_t | \mathbf{x}_0, z)\|_2^2 \right] + C_2.\end{aligned}$$

We get the result of Eq. (8).

#### B.5 DERIVATION OF REMARK 1

Although this result follows directly from prior studies (Vincent, 2011; Song & Ermon, 2019), we provide a brief derivation here for completeness. Let  $\mathcal{L}_{\text{DSM}}(\theta; q(X, Y))$  and  $\mathcal{L}_{\text{ESM}}(\theta; q(X, Y))$  denote

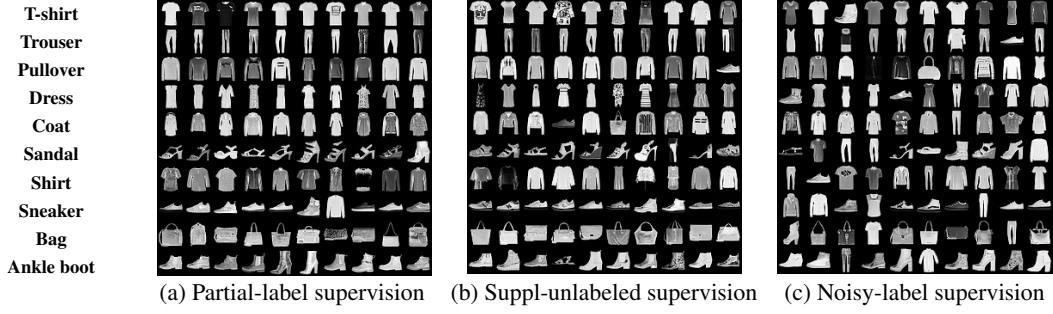


Figure 3: Examples of randomly generated Fashion-MNIST images from *Vanilla* models trained under different types of imprecise supervision.

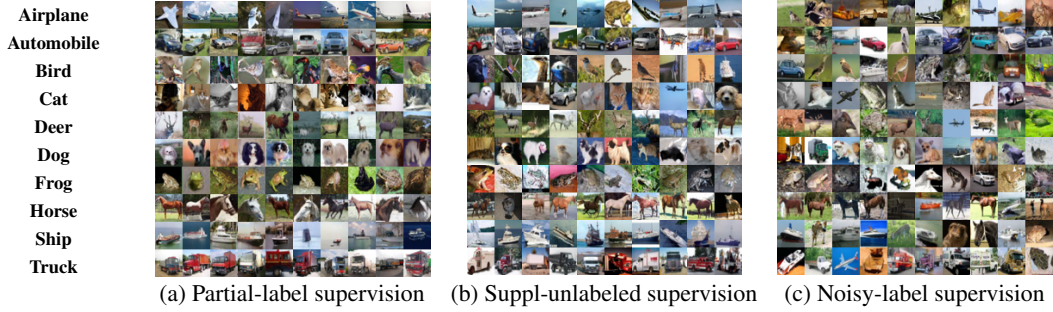


Figure 4: Examples of randomly generated CIFAR-10 images from *Vanilla* models trained under different types of imprecise supervision.

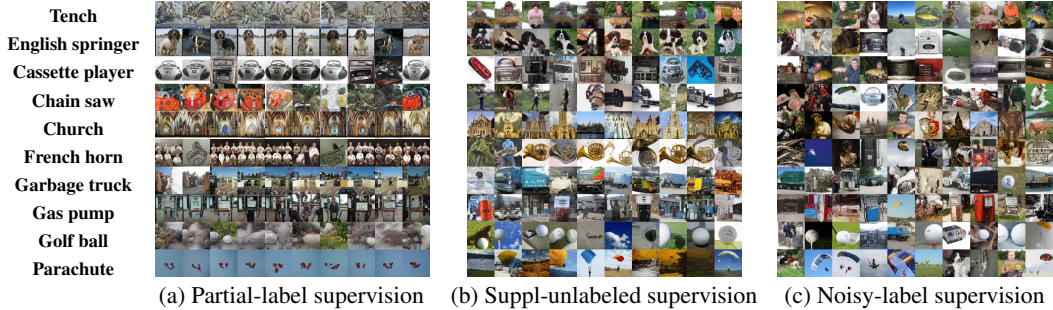


Figure 5: Examples of randomly generated ImageNette images from *Vanilla* models trained under different types of imprecise supervision.

the denoising score matching (DSM) and explicit score matching (ESM) objectives, respectively:

$$\mathcal{L}_{\text{DSM}}(\theta; q(X, Y)) := \mathbb{E}_t \left[ \lambda(t) \mathbb{E}_{y \sim q(Y)} \mathbb{E}_{\mathbf{x}_t \sim q_t(\mathbf{x}_t | \mathbf{x}, y)} \left\| \mathbf{s}_\theta(\mathbf{x}_t, y, t) - \nabla_{\mathbf{x}_t} \log q_{t|0}(\mathbf{x}_t | \mathbf{x}, Y = y) \right\|_2^2 \right],$$

$$\mathcal{L}_{\text{ESM}}(\theta; q(X, Y)) := \mathbb{E}_t \left[ \lambda(t) \mathbb{E}_{y \sim q(Y)} \mathbb{E}_{\mathbf{x}_t \sim q_t(\mathbf{x}_t | y)} \left\| \mathbf{s}_\theta(\mathbf{x}_t, y, t) - \nabla_{\mathbf{x}_t} \log q_t(\mathbf{x}_t | Y = y) \right\|_2^2 \right].$$

It has been established (Vincent, 2011; Song & Ermon, 2019) that these two formulations differ only by an additive constant independent of  $\theta$ :

$$\mathcal{L}_{\text{ESM}}(\theta; q(X, Y)) = \mathcal{L}_{\text{DSM}}(\theta; q(X, Y)) + C_3,$$

where  $C_3$  does not depend on  $\theta$ . Hence, both objectives admit the same minimizer.

Applying this result to an imprecise-label dataset by identifying  $Y = Z$ , let  $\theta_{\text{ESM}}^* := \arg \min_{\theta} \mathcal{L}_{\text{ESM}}(\theta; q(X, Z))$ . Then the optimal score function satisfies  $\mathbf{s}_{\theta_{\text{ESM}}^*}(\mathbf{x}_t, z, t) = \nabla_{\mathbf{x}_t} \log q_t(\mathbf{x}_t | Z = z)$ . Since the same conclusion holds for  $\mathcal{L}_{\text{DSM}}$ , we obtain  $\mathbf{s}_{\theta_{\text{ESM}}^*} = \mathbf{s}_{\theta_{\text{DSM}}^*} = \nabla_{\mathbf{x}_t} \log q_t(\mathbf{x}_t | z)$ , which is precisely the statement of Remark 1.

To directly illustrate this bias, we train CDMs under different forms of imprecise supervision by applying Eq. (8) directly, a baseline we refer to as *Vanilla*. We then visualize the images generated by these biased models, as shown in the figures below. The results reveal the following patterns:

- **Partial-label supervision:** The generated images often lack diversity and typically capture only the dominant object. This effect is particularly pronounced on the ImageNette dataset, where samples within the same class appear highly similar. Interestingly, the generated categories generally align with the ground-truth labels, suggesting that diffusion models can still extract correct class information under partial-label supervision. However, the inherent label ambiguity prevents the model from capturing intra-class variation.
- **Noisy-label supervision:** The generated samples tend to contain visual noise. Although the model is able to capture class diversity, corrupted labels cause mismatches between generated samples and their true categories.
- **Supplementary-unlabeled supervision:** The generated images are often both less diverse and noisier. This phenomenon combines the limitations of partial-label supervision with the challenge of abundant unlabeled samples. Because the model has limited access to labeled examples, it relies on averaging confidence across all classes, which reduces its discriminative boundaries and introduces noise.

## B.6 PROOF OF THEOREM 1

First, for all  $t$ , the perturbed distribution  $q_t(\mathbf{x}_t|z)$  satisfied:

$$q_t(\mathbf{x}_t|z) = \sum_{y=1}^c p(y|z)q_t(\mathbf{x}_t|y) \quad \forall \mathbf{x}_t \in \mathcal{X}, z \in \mathcal{Y}.$$

This implies that the transition from imprecise labels to clean labels is independent of the timesteps. Consequently, Eq. (9) can be derived as follows,

$$\begin{aligned} & \nabla_{\mathbf{x}_t} \log q_t(\mathbf{x}_t|z) \\ &= \frac{\nabla_{\mathbf{x}_t} q_t(\mathbf{x}_t|z)}{q_t(\mathbf{x}_t|z)} \\ &= \frac{\sum_{y=1}^c p(y|z) \nabla_{\mathbf{x}_t} q_t(\mathbf{x}_t|y)}{q_t(\mathbf{x}_t|z)} \\ &= \sum_{y=1}^c \frac{p(y|z)q_t(\mathbf{x}_t|y)}{q_t(\mathbf{x}_t|z)} \cdot \frac{\nabla_{\mathbf{x}_t} q_t(\mathbf{x}_t|y)}{q_t(\mathbf{x}_t|y)} \\ &= \sum_{y=1}^c \frac{p(y|z)q_t(\mathbf{x}_t|y)}{q_t(\mathbf{x}_t|z)} \cdot \nabla_{\mathbf{x}_t} \log q_t(\mathbf{x}_t|y) \\ &= \sum_{y=1}^c p(y|z) \cdot \frac{p(z)}{p(y)} \cdot \frac{p(y|\mathbf{x}_t)}{p(z|\mathbf{x}_t)} \cdot \frac{q_t(\mathbf{x}_t)}{q_t(\mathbf{x}_t)} \cdot \nabla_{\mathbf{x}_t} \log q_t(\mathbf{x}_t|y) \\ &= \sum_{y=1}^c p(z|y) \cdot \frac{p(y|\mathbf{x}_t)}{p(z|\mathbf{x}_t)} \cdot \nabla_{\mathbf{x}_t} \log q_t(\mathbf{x}_t|y) \\ &= \sum_{y=1}^c p(z|y, \mathbf{x}_t) \cdot \frac{p(y|\mathbf{x}_t)}{p(z|\mathbf{x}_t)} \cdot \nabla_{\mathbf{x}_t} \log q_t(\mathbf{x}_t|y) \quad (\text{Conditional indep. of } z \text{ and } \mathbf{x}_t \text{ given } y.) \\ &= \sum_{y=1}^c \frac{p(z|y, \mathbf{x}_t)p(y|\mathbf{x}_t)}{p(z|\mathbf{x}_t)} \cdot \nabla_{\mathbf{x}_t} \log q_t(\mathbf{x}_t|y) \\ &= \sum_{y=1}^c p(y|\mathbf{x}_t, z) \nabla_{\mathbf{x}_t} \log q_t(\mathbf{x}_t|y) \end{aligned}$$

### B.7 PROOF OF PROPOSITION 1

By Remark 1 and Theorem 1, the optimal solution  $\theta_{\text{Gen}}^*$  to Eq. (10) satisfies

$$\sum_{y=1}^c p(y|\mathbf{x}_t, z) \mathbf{s}_{\theta_{\text{Gen}}^*}(\mathbf{x}_t, y, t) = \nabla_{\mathbf{x}_t} \log q_t(\mathbf{x}_t|z) = \sum_{y=1}^c p(y|\mathbf{x}_t, z) \nabla_{\mathbf{x}_t} \log q_t(\mathbf{x}_t|y),$$

for all  $\mathbf{x}_t \in \mathcal{X}$ ,  $z \subseteq \mathcal{Y}$ , and  $t \in [T]$ .

Next, recall the weighted denoising score matching loss:

$$\mathcal{L}_{\text{Gen}}(\theta) = \mathbb{E}_t \left[ w_t \left\| \sum_{y=1}^c p(y|\mathbf{x}_t, z) \mathbf{s}_{\theta}(\mathbf{x}_t, y, t) - \sum_{y=1}^c p(y|\mathbf{x}_t, z) \nabla_{\mathbf{x}_t} \log q_t(\mathbf{x}_t|y) \right\|_2^2 \right].$$

Differentiating with respect to  $\mathbf{s}_{\theta}(\mathbf{x}_t, y, t)$  and setting the derivative to zero yields

$$\frac{\partial}{\partial \mathbf{s}_{\theta}(\mathbf{x}_t, y, t)} \mathcal{L}_{\text{Gen}}(\theta) = 2w_t p(y|\mathbf{x}_t, z) (\mathbf{s}_{\theta_{\text{Gen}}^*}(\mathbf{x}_t, y, t) - \nabla_{\mathbf{x}_t} \log q_t(\mathbf{x}_t|y)) = 0.$$

Since  $w_t > 0$ , for any  $y$  such that  $p(y|\mathbf{x}_t, z) > 0$ , the optimality condition implies

$$\mathbf{s}_{\theta_{\text{Gen}}^*}(\mathbf{x}_t, y, t) = \nabla_{\mathbf{x}_t} \log q_t(\mathbf{x}_t|y).$$

In particular, under the partial-label learning setting, if  $p(y|\mathbf{x}_t, z) = 0$ , the loss does not depend on  $\mathbf{s}_{\theta}(\mathbf{x}_t, y, t)$ , and the equality can be established without loss of generality. This completes the proof.

### B.8 PROOF OF THEOREM 2

We first consider the case where the timestep  $\tau$  is sampled from a log-normal distribution, as defined in the EDM framework. Specifically,

$$\ln(\tau) \sim \mathcal{N}(P_{\text{mean}}, P_{\text{std}}^2),$$

where the parameters are set to  $P_{\text{mean}} = 1.2$  and  $P_{\text{std}} = -1.2$ . Accordingly, the probability density function of  $\tau$  is given by

$$p(\tau) = \frac{1}{\tau P_{\text{std}} \sqrt{2\pi}} \exp\left(-\frac{(\ln \tau - P_{\text{mean}})^2}{2P_{\text{std}}^2}\right), \quad \tau > 0.$$

The corresponding cumulative distribution function (CDF) is denoted as:

$$F(\tau) = \frac{1}{2} \left[ 1 + \operatorname{erf}\left(\frac{\ln \tau - P_{\text{mean}}}{P_{\text{std}} \sqrt{2}}\right) \right],$$

where  $\operatorname{erf}(x)$  denotes the error function.

The median of this distribution  $\tau_{\text{mid}}$  is the value at which the CDF equals 0.5, i.e.,  $F(\tau_{\text{mid}}) = 0.5$ .

To ensure that the selected subinterval allows signal-dominant early timesteps and noise-dominant later timesteps to complement each other, we require the cumulative probability mass on either side of the median to be equal. Formally, for subinterval boundaries  $(l, r)$  with  $r = l + \Delta$ , we enforce the following symmetry condition:

$$F(r) - F(\tau_{\text{mid}}) = F(\tau_{\text{mid}}) - F(l).$$

Rewriting this with  $r = l + \Delta$  gives:

$$F(l + \Delta) + F(l) = 2F(\tau_{\text{mid}}) = 1.$$

This implicit equation defines the subinterval  $(l, l + \Delta)$  such that the cumulative probability mass is centered around the median of  $p(\tau)$ . To compute the left boundary  $l$ , we solve:

$$l = \operatorname{Solve}_{\tau} (F(\tau) + F(\tau + \Delta) - 1 = 0), \quad (21)$$

and set  $r = l + \Delta$ . The solution can be obtained using any standard root-finding algorithm, such as the Brent method (Brent, 2013).

We then consider the DDPM setting, where the timestep  $\tau$  is uniformly sampled from a fixed interval. Specifically, we assume  $\tau \sim \mathcal{U}(0, 1)$ , whose CDF is given by

$$F(\tau) = \tau$$

Under this distribution, the symmetry condition in Eq. (21) simplifies to

$$\begin{aligned} l &= \text{Solve}_\tau (F(\tau) + F(\tau + \Delta) - 1 = 0) \\ &= \text{Solve}_\tau (\tau + \tau + \Delta - 1 = 0) \\ &= \frac{1 - \Delta}{2}, \end{aligned}$$

and thus  $r = l + \Delta = \frac{1+\Delta}{2}$ . This result implies that the optimal subinterval is symmetric around the midpoint of the distribution. In the special case where only a single timestep is used (i.e.,  $\Delta \rightarrow 0$ ), the best estimate of the conditional ELBO occurs exactly at the median. As the sampled timestep deviates further from the midpoint, classification accuracy tends to degrade. This observation aligns with the empirical findings of Li et al. (2023), who reported that classification accuracy is maximized near the median and declines towards the edges. Their use of evenly spaced timesteps centered around the median further supports our strategy.

### B.9 PROOF OF THEOREM 3

For clarity, we abbreviate  $\bar{h}(\tau, y)$  as  $\bar{h}(\tau)$ , since the proof does not depend explicitly on  $y$ . Define the weighted integral of  $\bar{h}$  and the normalization factor over an interval  $[l, r]$  as

$$A(l, r) := \int_l^r \bar{h}(\tau) p(\tau) d\tau, \quad Z(l, r) := \int_l^r p(\tau) d\tau,$$

so that the local expectation can be written as  $\mu' = A(l, r)/Z(l, r)$ . Let  $\mu'' = \mathbb{E}_{\tau \sim p(\tau)}[\bar{h}(\tau)]$  denote the global expectation. The squared error objective in Eq. (16) then becomes

$$g(l, r) := (\mu' - \mu'')^2,$$

subject to the probability-mass constraint  $Z(l, r) = \alpha$ .

We apply the method of Lagrange multipliers with

$$L(l, r, \lambda) := (\mu' - \mu'')^2 + \lambda \left( \int_l^r p(\tau) d\tau - \alpha \right).$$

By the Leibniz rule, the derivatives of  $A(l, r)$  and  $Z(l, r)$  with respect to the interval boundaries are

$$\frac{\partial A(l, r)}{\partial l} = -\bar{h}(l) p(l), \quad \frac{\partial A(l, r)}{\partial r} = \bar{h}(r) p(r), \quad \frac{\partial Z(l, r)}{\partial l} = -p(l), \quad \frac{\partial Z(l, r)}{\partial r} = p(r).$$

Hence, the derivatives of  $\mu' = A/Z$  are

$$\frac{\partial \mu'}{\partial l} = \frac{p(l)}{Z(l, r)} (\mu' - \bar{h}(l)), \quad \frac{\partial \mu'}{\partial r} = \frac{p(r)}{Z(l, r)} (\bar{h}(r) - \mu').$$

Differentiating  $L$  w.r.t.  $l$  and  $r$  gives

$$\begin{aligned} \frac{\partial L}{\partial l} &= 2(\mu' - \mu'') \cdot \frac{p(l)}{Z(l, r)} (\mu' - \bar{h}(l)) - \lambda p(l), \\ \frac{\partial L}{\partial r} &= 2(\mu' - \mu'') \cdot \frac{p(r)}{Z(l, r)} (\bar{h}(r) - \mu') + \lambda p(r). \end{aligned}$$

Setting both derivatives to zero yields the necessary conditions

$$2(\mu' - \mu'')(\mu' - \bar{h}(l)) = \lambda Z(l, r), \quad 2(\mu' - \mu'')(\bar{h}(r) - \mu') = \lambda Z(l, r).$$

Equating the two expressions gives

$$\mu' - \bar{h}(l) = \bar{h}(r) - \mu' \implies \mu' = \frac{1}{2}(\bar{h}(l) + \bar{h}(r)).$$

Substituting back, we obtain

$$\int_l^r p(\tau) \bar{h}(\tau, y) d\tau = \frac{Z(l, r)}{2} (\bar{h}(l, y) + \bar{h}(r, y)), \quad Z(l, r) := \int_l^r p(\tau) d\tau.$$

Equivalently, the necessary optimality condition is  $\text{ERR}(l^*, r^*, y) = 0$ . Since  $Z(l^*, r^*) > 0$ , this is also equivalent to

$$\text{ERR}(l^*, r^*, y) := \mathbb{E}_{\tau \sim p(\tau | \tau \in [l^*, r^*])} [\bar{h}(\tau, y)] - \frac{1}{2} (\bar{h}(l^*, y) + \bar{h}(r^*, y)) = 0.$$

This establishes the necessary condition for an optimal subinterval.

## C DISCUSSION

### C.1 ANALYSIS OF EARLY-LEARNING REGULARIZATION IN EQ. (15)

The effectiveness of Eq. (15) can be better understood by examining the form of its gradient. For clarity, we restate the loss with the following notation: given a noisy-labeled input  $(\mathbf{x}, \hat{y})$ , we denote the model's output probabilities as  $f_\theta(\mathbf{x})$  and the corresponding EMA target as  $f_\phi(\mathbf{x})$ .

Let  $\hat{\mathbf{y}} \in \mathbb{R}^c$  be the one-hot vector corresponding to the noisy label  $\hat{y}$ . Then the loss over the whole dataset  $\mathcal{D} = \{(\mathbf{x}^{[i]}, \hat{\mathbf{y}}^{[i]})\}_{i=1}^n$  can be computed according to Eq. (15) as

$$\mathcal{L}_{\text{Cls}}^{\text{NL}}(\mathcal{D}) = -\frac{1}{n} \sum_{i=1}^n \langle \text{sg}(\mathbf{r}^{[i]}), \log f_\theta(\mathbf{x}^{[i]}) \rangle, \quad \mathbf{r}^{[i]} = \hat{\mathbf{y}}^{[i]} - \lambda \frac{f_\theta(\mathbf{x}^{[i]}) \odot (\delta^{[i]} \mathbf{1} - f_\phi(\mathbf{x}^{[i]}))}{1 - \delta^{[i]}}, \quad (22)$$

where  $\delta^{[i]} = \langle f_\theta(\mathbf{x}^{[i]}), f_\phi(\mathbf{x}^{[i]}) \rangle$ ,  $\text{sg}(\cdot)$  denotes the stop-gradient operator, and  $\odot$  is the Hadamard product. By construction  $\mathbf{r}^{[i]}$  is treated as a *constant* w.r.t.  $\theta$  due to the stop-gradient.

**Lemma 1.** *Let  $\psi_\theta(\mathbf{x})$  denote the pre-softmax logits such that  $f_\theta(\mathbf{x}) = \text{softmax}(\psi_\theta(\mathbf{x}))$ . For the loss in Eq. (15), the gradients are*

$$\frac{\partial \mathcal{L}_{\text{Cls}}^{\text{NL}}(\mathbf{x}^{[i]})}{\partial \psi_\theta(\mathbf{x}^{[i]})} = f_\theta(\mathbf{x}^{[i]}) - \text{sg}(\mathbf{r}^{[i]}), \quad \text{for each } i = 1, \dots, n, \quad (23)$$

and, by the chain rule,

$$\nabla_\theta \mathcal{L}_{\text{Cls}}^{\text{NL}}(\mathcal{D}) = \frac{1}{n} \sum_{i=1}^n J_{\mathbf{z}_\theta}(\mathbf{x}^{[i]})^\top \left[ f_\theta(\mathbf{x}^{[i]}) - \text{sg}(\mathbf{r}^{[i]}) \right], \quad (24)$$

where  $J_{\mathbf{z}_\theta}(\mathbf{x}) = \partial \mathbf{z}_\theta(\mathbf{x}) / \partial \theta$  is the Jacobian of the logits w.r.t. the parameters. Equivalently, expanding  $\mathbf{r}^{[i]}$  gives

$$\nabla_\theta \mathcal{L}_{\text{Cls}}^{\text{NL}}(\mathcal{D}) = \frac{1}{n} \sum_{i=1}^n J_{\mathbf{z}_\theta}(\mathbf{x}^{[i]})^\top \left[ f_\theta(\mathbf{x}^{[i]}) - \hat{\mathbf{y}}^{[i]} + \lambda \text{sg} \left( \frac{f_\theta(\mathbf{x}^{[i]}) \odot (\delta^{[i]} \mathbf{1} - f_\phi(\mathbf{x}^{[i]}))}{1 - \delta^{[i]}} \right) \right]. \quad (25)$$

*Proof.* For any  $i \in \{1, \dots, n\}$ , let us first verify that  $\mathbf{r}^{[i]}$  sums to 1. With

$$\mathbf{r}^{[i]} = \hat{\mathbf{y}}^{[i]} - \lambda \frac{f_\theta(\mathbf{x}^{[i]}) \odot (\delta^{[i]} \mathbf{1} - f_\phi(\mathbf{x}^{[i]}))}{1 - \delta^{[i]}},$$

we sum over classes and using  $\langle f_\theta(\mathbf{x}^{[i]}), \mathbf{1} \rangle = 1$  yields

$$\mathbf{1}^\top \mathbf{r}^{[i]} = 1 - \lambda \frac{\delta^{[i]} - \langle f_\theta(\mathbf{x}^{[i]}), f_\phi(\mathbf{x}^{[i]}) \rangle}{1 - \delta^{[i]}} = 1,$$

so  $\mathbf{r}^{[i]}$  lies on the simplex (hence Eq. (22) is an ordinary cross-entropy with a fixed target). Let  $\psi^{[i]} = \psi_\theta(\mathbf{x}^{[i]})$  be the logits and recall  $\frac{\partial \log \text{softmax}(\psi)}{\partial \psi} = I - \text{softmax}(\psi) \mathbf{1}^\top$ . For the per-sample loss  $\ell^{[i]} = -\langle \text{sg}(\mathbf{r}^{[i]}), \log \text{softmax}(\psi^{[i]}) \rangle$ , the derivative w.r.t. logits is

$$\frac{\partial \ell^{[i]}}{\partial \psi^{[i]}} = \text{softmax}(\psi^{[i]}) - \text{sg}(\mathbf{r}^{[i]}) = f_\theta(\mathbf{x}^{[i]}) - \text{sg}(\mathbf{r}^{[i]}),$$

which is Eq. (23). Applying the chain rule and averaging over  $i$  gives Eq. (24). Replacing  $\text{sg}(\mathbf{r}^{[i]})$  by its explicit form produces Eq. (25).  $\square$

**Remark.** Eq. (25) shows that  $\mathcal{L}_{\text{Cls}}^{\text{NL}}$  behaves like the standard cross-entropy gradient plus an ELR-like corrective term. This term amplifies gradients on clean samples and counteracts gradients on noisy samples. Specifically, we expand this ELR-like corrective term into:

$$\mathbf{g}_y^{[z]} := \frac{f_\theta(\mathbf{x}^{[z]})}{1 - \langle f_\theta(\mathbf{x}^{[z]}), f_\phi(\mathbf{x}^{[z]}) \rangle} \sum_{k=1}^c (f_\phi(\mathbf{x}^{[z]})_k - f_\phi(\mathbf{x}^{[z]})_y) f_\theta(\mathbf{x}^{[z]})_k. \quad (26)$$

If  $y^*$  is the true class, then the  $y^*$ -th entry of  $f_\phi(\mathbf{x}^{[z]})$  tends to be dominant during early-learning. In that case, the  $y^*$ -th entry of  $\mathbf{g}^{[z]}$  is negative. This is useful both for examples with clean labels and for examples with noisy labels. For examples with clean labels, the cross-entropy term  $f_\theta(\mathbf{x}^{[z]}) - \hat{y}^{[z]}$  tends to vanish after the early-learning stage because  $f_\theta(\mathbf{x}^{[z]})$  is very close to  $\hat{y}^{[z]}$ , allowing examples with wrong labels to dominate the gradient. Adding  $\mathbf{g}^{[z]}$  counteracts this effect by ensuring that the magnitudes of the coefficients on examples with clean labels remain large. Thus,  $\mathbf{g}^{[z]}$  fulfils the two desired properties that boosting the gradient of examples with clean labels, and neutralizing the gradient of the examples with false labels.

## C.2 CLASS-PRIOR ESTIMATION IN IMPRECISE-LABEL DATASETS

When the class priors  $p(y)$  (here we slightly abuse notation and denote them as  $\pi_y$ ) are not directly accessible to the learning algorithm, they can be estimated using off-the-shelf estimation methods (Luo et al., 2024; Wang et al., 2022a). In this section, we present the problem formulation and outline how class priors can be estimated in practice.

### C.2.1 CLASS-PRIOR ESTIMATION IN PARTIAL-LABEL DATASETS

In partial-label learning, each instance is associated with a candidate label set rather than a single ground-truth label. This label ambiguity makes it difficult to estimate the class prior distribution, since simply counting training samples per class is no longer feasible. To address this issue, we adopt an iterative estimation strategy that updates the class prior in a moving-average manner.

We use the model’s predicted labels as a proxy for class prior estimation. Since predictions in the early stage of training are often unreliable, we design a moving-average update rule that gradually stabilizes the estimated distribution. The update starts from a uniform prior  $\mathbf{r} = [1/c, \dots, 1/c]$ , and is refined at each training epoch as

$$\mathbf{r} \leftarrow \mu \mathbf{r} + (1 - \mu) \mathbf{z}, \quad \mathbf{z}_j = \frac{1}{n} \sum_{i=1}^n \mathbb{I} \left( j = \arg \max_{y \in S_i} f_j(x_i) \right), \quad (27)$$

where  $\mu \in [0, 1]$  is a momentum parameter,  $S_i$  is the candidate label set for sample  $x_i$ , and  $f_j(x_i)$  denotes the model prediction for class  $j$ . This rule progressively refines  $\mathbf{r}$  as the model improves, leading to more accurate and stable class-prior estimates.

### C.2.2 CLASS-PRIOR ESTIMATION IN SUPPLEMENTARY-UNLABELED DATASETS

In the case of supplementary-unlabeled datasets, which also is called semi-supervised datasets, the estimation of class-prior is relatively straightforward. We assume that the distribution of the labeled dataset is consistent with that of the unlabeled dataset. Therefore, the class-prior can be directly obtained by counting the class distribution over the labeled dataset, which serves as a reliable approximation of the overall data distribution.

### C.2.3 CLASS-PRIOR ESTIMATION IN NOISY-LABEL DATASETS

We consider the widely adopted class-dependent label noise setting (Yao et al., 2020), where the observed noisy label of each  $\mathbf{x} \in \mathcal{X}$  depends only on its underlying clean label. Formally, the transition probability from class  $i$  to class  $j$  is defined as

$$P(\tilde{Y} = e_j | Y = e_i, X = \mathbf{x}) = P(\tilde{Y} = e_j | Y = e_i) = T_{ij}, \quad \forall i, j \in [[c]],$$

where  $\mathbf{T} = [T_{ij}] \in [0, 1]^{c \times c}$  is the noise transition matrix. To make the estimation of  $\mathbf{T}$  feasible, we follow prior work and impose the following assumptions.

**Assumption 1** (Sufficiently Scattered Assumption (Li et al., 2021b)). The clean class posterior  $P(Y | X) = [P(Y = e_1 | X), \dots, P(Y = e_c | X)]^\top \in [0, 1]^c$  is said to be sufficiently scattered if there exists a set  $\mathcal{H} = \{\mathbf{x}_1, \dots, \mathbf{x}_m\}$  such that the matrix  $\mathbf{H} = [P(Y | X = \mathbf{x}_1), \dots, P(Y | X = \mathbf{x}_m)]$  satisfies: (i)  $\mathcal{Q} \subseteq \text{cone}\{\mathbf{H}\}$ , where  $\mathcal{Q} = \{\mathbf{v} \in \mathbb{R}^c \mid \mathbf{v}^\top \mathbf{1} \geq \sqrt{c-1} \|\mathbf{v}\|_2\}$ , and  $\text{cone}\{\mathbf{H}\}$  denotes the convex cone generated by the columns of  $\mathbf{H}$ ; (ii)  $\text{cone}\{\mathbf{H}\} \not\subseteq \text{cone}\{\mathbf{U}\}$  for any unitary matrix  $\mathbf{U} \in \mathbb{R}^{c \times c}$  that is not a permutation matrix.

**Assumption 2** (Nonsingular  $\mathbf{T}$ ). The transition matrix  $\mathbf{T}$  is nonsingular, i.e.,  $\text{Rank}(\mathbf{T}) = c$ .

Assumption 1 ensures that the clean posteriors are sufficiently scattered so that the ground-truth  $\mathbf{T}$  can be identified, while Assumption 2 guarantees the invertibility of  $\mathbf{T}$ .

Let  $\epsilon$  denote the noise rate. For symmetric label noise, we have  $T_{ii} = 1 - \epsilon$  and  $T_{ij} = \frac{\epsilon}{c-1}$  with  $j \neq i$ . In practice, the transition matrix can be estimated by solving the following optimization problem (Li et al., 2021b):

$$\min_{\theta, \hat{\mathbf{T}}} L(\theta, \hat{\mathbf{T}}) = \frac{1}{n} \sum_{i=1}^n \ell(\hat{\mathbf{T}}^\top h_\theta(\mathbf{x}_i), \tilde{y}_i) + \lambda \cdot \log \det(\hat{\mathbf{T}}), \quad (28)$$

where  $\ell$  is a loss function (typically cross-entropy),  $h_\theta(\cdot)$  is the output of a neural network parameterized by  $\theta$ , and the regularization term  $\log \det(\hat{\mathbf{T}})$  encourages the estimated transition matrix to have minimal simplex volume. Here  $\lambda > 0$  is a trade-off hyperparameter. By Assumption 1, the solution  $\hat{\mathbf{T}}$  converges to the true  $\mathbf{T}$  given sufficient noisy data (Theorem 1 in (Li et al., 2021b)).

Once the transition matrix  $\mathbf{T}$  is estimated, the clean class prior  $\pi = [\pi_1, \dots, \pi_c]^\top$  can be obtained by solving the following system of linear equations:

$$\begin{cases} \tilde{\pi}_1 = T_{11}\pi_1 + T_{21}\pi_2 + \dots + T_{c1}\pi_c \\ \tilde{\pi}_2 = T_{12}\pi_1 + T_{22}\pi_2 + \dots + T_{c2}\pi_c \\ \vdots \\ \tilde{\pi}_c = T_{1c}\pi_1 + T_{2c}\pi_2 + \dots + T_{cc}\pi_c \end{cases}, \quad (29)$$

where  $\tilde{\pi}_i = P(\tilde{Y} = e_i)$  is the noisy class prior of the  $i$ -th class. The empirical estimate of  $\tilde{\pi}_i$  can be computed as

$$\hat{\tilde{\pi}}_i = \frac{1}{n} \sum_{j=1}^n \mathbf{1}\{\tilde{y}_j = e_i\}, \quad \forall i \in [c]. \quad (30)$$

Solving this system yields the clean class prior  $\pi$ , which is then used in subsequent modeling.

## D IMPLEMENTATION DETAILS

Our implementation is based on PyTorch 1.12 (Paszke et al., 2019), and all experiments were conducted on NVIDIA Tesla A100 GPUs with CUDA 12.4.

**Imprecise-label construction.** For all class-dependent partial-label datasets, we construct a

$$10 \times 10 \text{ circulant transition matrix } \begin{bmatrix} 1 & q+0.2 & q & q-0.2 & \dots & q+0.2 & q & q-0.2 \\ q-0.2 & 1 & q+0.2 & q & \dots & q & q-0.2 & q+0.2 \\ q & q-0.2 & 1 & q+0.2 & \dots & q-0.2 & q+0.2 & q \\ \vdots & \vdots & \vdots & \vdots & \ddots & \vdots & \vdots & \vdots \\ q+0.2 & q & q-0.2 & 1 & \dots & q & q-0.2 & 1 \end{bmatrix}, \text{ where}$$

each row maps a true label to a candidate set of labels with varying probabilities, and  $q$  is set to 0.5. For noisy-label datasets with asymmetric noise (40% flip probability), we adopt the following mappings: *Fashion-MNIST*: ‘Pullover’→‘Sneaker’, ‘Dress’→‘Bag’, ‘Sandal’→‘Shirt’, ‘Shirt’→‘Sandal’. *CIFAR-10*: ‘Truck’→‘Automobile’, ‘Bird’→‘Airplane’, ‘Deer’→‘Horse’, ‘Cat’→‘Dog’, ‘Dog’→‘Cat’. *ImageNette*: ‘Tench’→‘English springer’, ‘Cassette player’→‘Garbage truck’, ‘Chain saw’→‘Church’, ‘Golf ball’→‘Parachute’, ‘Parachute’→‘Golf ball’.

**Model setup.** The overall diffusion framework follows EDM (Karras et al., 2022), and the training hyperparameters are kept consistent with those reported therein. For all experiments, we adopt the DDPM++ network architecture with a U-Net backbone. Specifically, we employ the Adam optimizer

with a learning rate of  $1e-3$ , parameters  $(\beta_1, \beta_2) = (0.9, 0.999)$ , and  $\epsilon = 1e-8$ . The EMA decay is set to 0.5. We use a batch size of 128 for Fashion-MNIST, 64 for CIFAR-10, and 16 for ImageNet. For the diffusion classifier, we set the timestep interval length  $\Delta$  to 6.4. All models are trained from scratch for 200k iterations.

## E EXPERIMENTS

### E.1 EVALUATION METRICS

We evaluate the trained CDMs using four unconditional metrics, including Fréchet Inception Distance (FID) (Heusel et al., 2017), Inception Score (IS) (Salimans et al., 2016), Density, and Coverage (Naeem et al., 2020), and three conditional metrics, namely CW-FID, CW-Density, CW-Coverage (Chao et al., 2022). All metrics are computed using the official implementation of DLSM (Chao et al., 2022). Although these metrics have been introduced in related work (Na et al., 2024), we briefly recap them here for completeness and clarity.

**Unconditional metrics.** Unconditional metrics evaluate generated samples without reference to class labels. In our experiments, images are first generated conditionally per class but then pooled without labels when computing the metrics. This evaluation protocol is consistent with prior studies (Kaneko et al., 2019; Chao et al., 2022).

- FID measures the distance between real and generated image distributions in the pre-trained feature space (Szegedy et al., 2016), indicating the fidelity and diversity of generated images.
- IS evaluates whether generated images belong to distinct classes and whether each image is class-consistent, reflecting the realism and class separability of generated images.
- Density and Coverage are reliable versions of Precision and Recall (Naeem et al., 2020), respectively. Density measures how well generated samples cover real data distribution, while Coverage assesses how well real samples are represented by generated ones.

**Conditional metrics.** To measure conditional consistency, we adopt class-wise (CW) variants of the above metrics, which compute each metric separately within each class and then average across classes. Notably, CW-FID (also called intra-FID) is widely used in conditional generative modeling (Miyato & Koyama, 2018; Kaneko et al., 2019), and has been highlighted as a key measure of conditional distribution quality.

**Remark:** It should be noted that the Fashion-MNIST dataset is not suitable for evaluation using these metrics, so we do not perform evaluation on the Fashion-MNIST dataset.

### E.2 FULL RESULTS IN WEAKLY SUPERVISED LEARNING

Building on the experiments presented in the main text, we further provide an extended comparison with a broader set of methods to ensure a comprehensive evaluation. The details are summarized as

**Partial-label learning.** We compare against ten representative baselines: *PRODEN* (Lv et al., 2020), *CAVL* (Zhang et al., 2021b), *POP* (Xu et al., 2023), *CC* (Feng et al., 2020), *LWS* (Wen et al., 2021), *IDGP* (Qiao et al., 2023), *PiCO* (Wang et al., 2023), *ABLE* (Xia et al., 2022), *CRDPLL* (Wu et al., 2022), and *DIRK* (Wu et al., 2024). For a fair comparison, we follow the hyperparameter settings used in *PLENCH* (Wang et al., 2025b). The complete results are reported in Table 5.

**Semi-supervised learning.** We follow the training and evaluation protocols of *USB* (Wang et al., 2022c), a widely adopted benchmark for fair and unified SSL comparisons. Our baselines cover a broad spectrum of recent approaches. First, we include confidence-thresholding methods such as *FixMatch* (Sohn et al., 2020), *FlexMatch* (Zhang et al., 2021a), *FreeMatch* (Wang et al., 2022d), *ReMixMatch* (Berthelot et al., 2019a), *Dash* (Xu et al., 2021) and *UDA* (Xie et al., 2020). Second, we consider contrastive-learning based and pseudo-label based methods, including *CoMatch* (Li et al., 2021a), *SoftMatch* (Chen et al., 2023) and *SimMatch* (Zheng et al., 2022). Finally, we add several classical and widely studied SSL approaches, including *Pseudo-Labeling* (Lee et al., 2013), *VAT* (Miyato et al., 2018) and *Mean Teacher* (Tarvainen & Valpola, 2017). This diverse collection of baselines allows us to rigorously examine whether our framework remains competitive against both state-of-the-art and classical SSL methods under consistent experimental setups.

Table 5: Classification results on Fashion-MNIST, CIFAR-10, and ImageNette datasets under various types of partial-label supervision. **Bold** numbers indicate the best performance.

Method	Fashion-MNIST		CIFAR-10		ImageNette	
	Random	Class-50%	Random	Class-50%	Random	Class-50%
<i>PRODEN</i>	93.31±0.07	93.44±0.21	90.02±0.22	90.44±0.44	84.75±0.13	83.50±0.60
<i>CAVL</i>	93.09±0.17	92.67±0.25	87.28±0.64	87.16±0.58	41.69±4.12	46.46±7.15
<i>POP</i>	93.59±0.17	93.57±0.19	89.13±0.22	90.19±0.10	84.65±0.55	84.29±0.17
<i>CC</i>	93.17±0.32	92.65±0.29	88.40±0.24	89.12±0.23	81.11±0.50	80.74±0.68
<i>IDGP</i>	92.26±1.25	93.07±0.16	89.65±0.53	90.83±0.34	84.07±0.26	82.18±0.13
<i>PiCO</i>	93.32±0.12	93.32±0.33	86.40±0.89	87.51±0.66	82.15±0.23	84.41±0.93
<i>ABLE</i>	93.02±0.26	93.20±0.16	90.77±0.33	90.74±0.48	71.81±2.46	76.53±1.28
<i>CRDPLL</i>	94.03±0.14	93.80±0.23	92.74±0.26	92.89±0.27	84.31±0.25	88.08±0.34
<i>DIRK</i>	94.11±0.22	93.99±0.24	93.48±0.14	93.22±0.37	87.90±0.11	87.47±0.17
<i>Vanilla</i>	80.20±1.29	66.03±1.43	60.25±0.17	56.34±0.50	56.04±0.61	59.47±0.51
<i>DMIS<sup>CE</sup></i>	84.24±0.37	78.45±0.46	91.47±0.15	90.52±0.35	84.49±0.05	82.34±0.27
<i>DMIS</i>	<b>94.27±0.55</b>	<b>94.20±0.15</b>	<b>94.70±0.49</b>	<b>93.53±0.12</b>	<b>89.31±0.21</b>	<b>88.42±0.43</b>

Table 6: Classification results on Fashion-MNIST, CIFAR-10, and ImageNette datasets under various types of supplementary-unlabeled supervision. **Bold** numbers indicate the best performance.

Method	Fashion-MNIST		CIFAR-10		ImageNette	
	Random-1%	Random-10%	Random-1%	Random-10%	Random-1%	Random-10%
<i>Pseudo-Labeling</i>	83.53±0.46	89.59±0.23	50.10±0.95	72.92±0.17	43.00±0.82	68.03±0.32
<i>Mean Teacher</i>	82.34±0.09	89.91±0.15	47.69±0.27	73.01±0.78	40.53±1.56	65.72±0.55
<i>VAT</i>	83.31±0.61	89.35±0.12	49.64±0.90	71.07±1.27	38.63±8.39	63.93±5.18
<i>UDA</i>	84.28±0.41	90.83±0.34	69.20±1.41	80.50±0.55	50.52±3.79	72.53±1.17
<i>FixMatch</i>	84.32±0.33	90.76±0.38	67.48±1.42	80.00±0.63	50.41±4.43	71.32±1.93
<i>Dash</i>	84.73±0.09	91.16±0.20	70.14±0.69	81.50±0.68	57.68±2.19	74.66±0.81
<i>CoMatch</i>	85.31±0.29	90.52±0.12	61.45±1.46	77.79±0.53	63.88±0.78	73.20±0.46
<i>FlexMatch</i>	84.43±0.30	90.69±0.03	70.72±0.93	81.35±0.48	61.39±0.70	73.08±0.13
<i>FreeMatch</i>	84.30±0.37	90.92±0.24	70.15±0.44	80.99±0.56	60.37±1.11	73.14±1.03
<i>SimMatch</i>	84.69±0.17	91.18±0.13	73.33±1.02	82.90±0.43	58.12±2.66	76.12±0.45
<i>SoftMatch</i>	84.72±0.23	91.22±0.11	73.24±0.82	88.66±0.60	58.50±2.31	75.75±0.25
<i>Vanilla</i>	78.37±3.72	90.50±1.00	53.49±0.15	85.13±0.12	49.55±0.99	74.70±0.53
<i>DMIS<sup>CE</sup></i>	82.92±0.17	91.07±0.18	75.40±0.54	89.85±0.08	62.64±0.24	71.39±0.45
<i>DMIS</i>	<b>85.92±0.13</b>	<b>92.97±0.21</b>	<b>76.30±0.17</b>	<b>92.47±0.39</b>	<b>68.23±0.19</b>	<b>77.30±0.15</b>

Table 7: Classification results on Fashion-MNIST, CIFAR-10, and ImageNette datasets under various types of noisy-label supervision. **Bold** numbers indicate the best performance.

Method	Fashion-MNIST		CIFAR-10		ImageNette	
	Sym-40%	Asym-40%	Sym-40%	Asym-40%	Sym-40%	Asym-40%
<i>CE</i>	76.18±0.26	82.01±0.06	67.22±0.26	76.98±0.42	58.43±0.77	71.81±0.38
<i>Co-learning</i>	90.85±0.63	84.10±2.01	84.97±0.53	80.36±1.09	76.16±0.96	75.37±0.49
<i>Co-teaching</i>	92.17±0.34	92.78±0.25	86.54±0.57	79.38±0.39	66.55±1.00	75.12±0.50
<i>Co-teaching+</i>	91.05±0.06	91.62±0.20	67.28±1.85	79.43±0.47	75.79±0.79	75.17±0.40
<i>SCE</i>	93.62±0.22	88.60±0.20	82.82±0.40	81.54±0.64	77.99±0.39	74.81±1.04
<i>GCE</i>	93.64±0.03	87.48±0.09	85.00±0.27	77.97±3.69	81.18±0.35	72.61±1.14
<i>Decoupling</i>	92.24±0.23	92.10±0.44	82.24±0.28	79.89±0.58	75.53±0.69	78.24±0.21
<i>ELR</i>	93.13±0.13	92.82±0.09	85.68±0.13	81.32±0.31	84.03±2.86	73.51±0.31
<i>JoCoR</i>	84.05±1.11	89.45±4.43	77.92±3.92	78.68±0.07	67.82±1.97	74.67±0.43
<i>Mixup</i>	92.21±0.03	92.01±1.02	84.26±0.64	83.21±0.85	76.65±1.62	77.16±0.71
<i>PENCIL</i>	90.85±0.58	91.77±0.69	85.91±0.26	84.89±1.49	81.94±1.26	77.20±1.15
<i>Vanilla</i>	90.11±1.24	85.41±0.96	80.22±0.10	86.31±0.10	55.86±1.95	53.91±1.07
<i>DMIS<sup>CE</sup></i>	82.76±0.57	83.39±0.24	84.75±0.36	84.21±0.18	80.47±0.56	77.21±0.19
<i>DMIS</i>	<b>93.40±0.40</b>	<b>93.20±0.30</b>	<b>88.63±0.12</b>	<b>88.83±0.33</b>	<b>84.12±0.18</b>	<b>79.30±0.27</b>

**Noisy-label learning.** We further benchmark our method against nine widely used approaches: *Coteaching* (Han et al., 2018), *Coteaching+* (Yu et al., 2019), *SCE* (Wang et al., 2019), *GCE* (Zhang & Sabuncu, 2018), *Decoupling* (Malach & Shalev-Shwartz, 2017), *ELR* (Liu et al., 2020), and *JoCoR* (Wei et al., 2020). These methods cover a range of strategies, from sample selection and reweighting to robust loss design, thus providing a diverse and rigorous benchmark.

Across all three weakly supervised scenarios, our method consistently achieves the best performance compared to existing baselines, reinforcing both its robustness and versatility under different forms of imprecise supervision.

### E.3 INTEGRATION WITH EXISTING IMPRECISE-LABEL CORRECTORS

Existing weakly supervised learning methods often rely on pseudo-labeling strategies that aim to correct imprecise labels by assigning refined labels to training samples. From this perspective, our approach is orthogonal to such methods: while pseudo-labeling seeks to approximate the true labels as closely as possible, our framework focuses on robustly learning from the remaining label noise. In practice, pseudo-labeling methods inevitably produce imperfect corrections. While most samples may be relabeled correctly, a non-negligible portion of instances still receive erroneous pseudo-labels because no classifier is perfect. As a result, imprecise supervision is effectively transformed into a noisy-label supervision.

This naturally complements our framework: by combining a pseudo-label corrector with *DMIS*, one can first reduce label uncertainty through correction and then leverage the robustness of diffusion models to learn from the residual noise. To validate this premise, we conduct a case study where a noisy-label learning method trained on CIFAR-10 with 40% symmetric noise achieves a pseudo-label accuracy of 80% on the training set. Using this pseudo-labeled dataset as input, our *DMIS* framework further improves the classification performance. As illustrated in Figure 6, integrating pseudo-label correction with *DMIS* consistently improves the performance across all datasets. Thus, we believe that our framework addresses the challenge of imprecise labels through the lens of diffusion model, offering a complementary perspective to conventional noisy-label approaches.

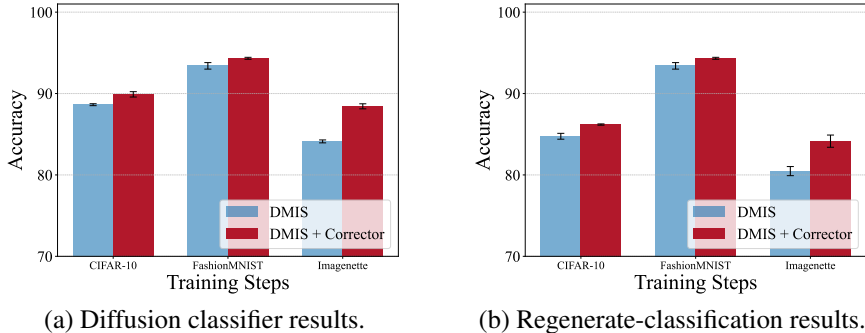


Figure 6: Test accuracy before and after applying pseudo-label correction with *DMIS*.

### E.4 COMPARISON OF ACCURACY CURVES BETWEEN *DMIS* AND *Vanilla*

To better illustrate the difference between the *Vanilla* method and our proposed *DMIS*, we plot the test accuracy curves during training, as shown in Figure 7. Across all settings, the *Vanilla* model exhibits an initial rise in accuracy followed by a gradual decline as training progresses, suggesting that it struggles to maintain stable performance under prolonged training. In contrast, *DMIS* consistently sustains high accuracy throughout training, showing its robustness across diverse supervision types.

Specifically, in the noisy-label setting, the decline of *Vanilla* is especially pronounced, reflecting its sensitivity to label corruption. In partial-label learning, *Vanilla* also exhibits instability, whereas *DMIS* maintains reliable performance. Even in semi-supervised learning, where labels are clean but scarce, *DMIS* achieves higher and more stable accuracy compared to *Vanilla*, demonstrating that our framework is not only noise-robust but also effective in leveraging limited supervision.

### E.5 VISUALIZATION OF NOISY CONDENSED DATASETS

We visualize the condensed images on CIFAR-10 and Fashion-MNIST in Figure 8 and Figure 9, respectively. It is evident that datasets generated by our method exhibit both higher diversity and stronger realism compared to other approaches. In particular, for the condensed Fashion-MNIST images, methods such as *DC* and *DM* often produce samples that do not faithfully correspond to their assigned class, resulting in condensed datasets that still contain noisy labels and thus degrade performance. By contrast, our proposed *DMIS* generates class-consistent and visually recognizable samples across categories, yielding condensed datasets that better preserve label fidelity and semantic

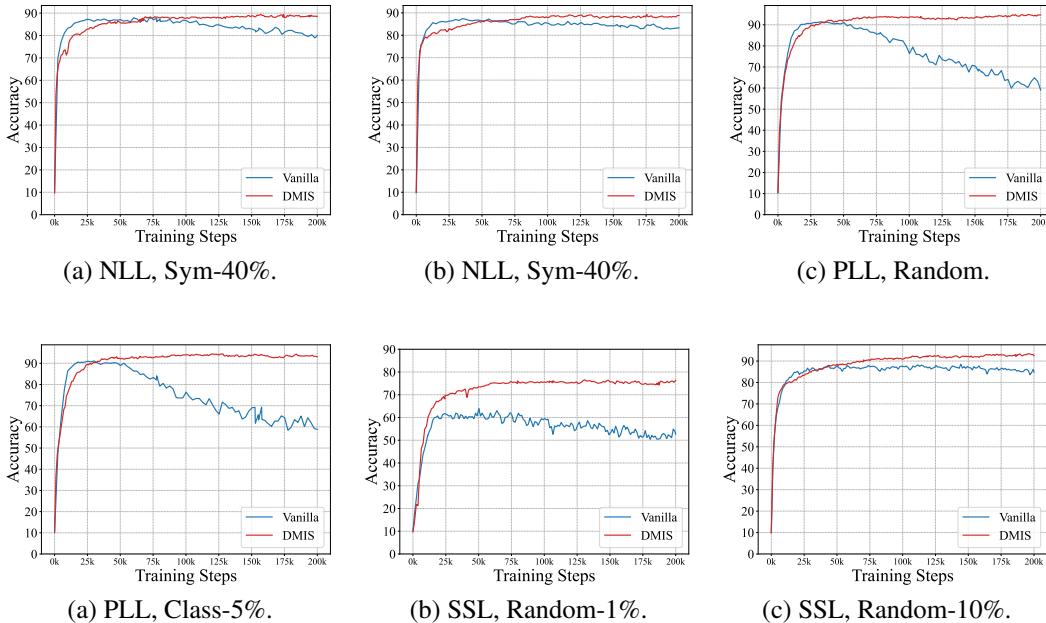


Figure 7: Test accuracy curves of the *Vanilla* and *DMIS* models on CIFAR-10 under different forms of imprecise supervision, including noisy-label learning (NLL), partial-label learning (PLL), and semi-supervised learning (SSL).

alignment. These visualizations further support the quantitative results, highlighting the advantage of generative condensation under noisy supervision.

### E.6 ADDITIONAL RESULTS ON DATASET CONDENSATION UNDER DIFFERENT FORMS OF IMPRECISE SUPERVISION

To illustrate the extreme case of noisy dataset condensation, we report the results when the IPC is set to 1. As shown in Table 8, *DMIS* consistently achieves the best performance across all datasets and noise types, even under the extreme case of  $IPC = 1$ . Notably, while most existing condensation methods collapse under severe supervision noise, our method maintains a clear advantage, outperforming the strongest baselines by a large margin. These results further demonstrate the robustness of *DMIS* in distilling informative representations despite highly limited and imprecisely labeled data.

Table 8: Classification results (test accuracy, %) on noisy-label Fashion-MNIST, CIFAR-10, and ImageNette datasets. ‘IPC’ indicates the number of images per class in the condensed dataset. **Bold** numbers indicate the best performance.

Dataset	Type	IPC	DC	DSA	DM	MTT	RDED	SRE2L	DMIS
F-MNIST	Sym-40%	1	15.21±0.75	19.55±0.58	15.56±0.20	10.86±1.90	18.07±3.33	14.33±1.20	<b>33.18±2.15</b>
	Asym-40%	1	20.17±0.29	17.61±0.89	23.91±0.36	7.39±0.84	13.20±0.83	13.13±0.21	<b>25.78±0.70</b>
CIFAR-10	Sym-40%	1	8.99±1.59	10.00±0.00	<b>14.41±1.03</b>	9.99±0.00	11.20±0.41	11.06±0.83	11.81±1.04
	Asym-40%	1	11.88±1.55	10.00±0.00	10.00±0.00	9.96±0.05	13.96±1.38	15.49±0.34	<b>15.88±0.57</b>
ImageNette	Sym-40%	1	9.87±0.00	9.87±0.00	9.87±0.00	19.17±2.35	12.98±1.16	11.90±0.78	<b>19.32±0.84</b>
	Asym-40%	1	9.87±0.00	9.87±0.00	9.87±0.00	17.36±0.10	12.98±0.42	18.55±2.19	<b>21.13±0.95</b>

Furthermore, even when samples are imprecisely annotated with candidate labels, our method is still able to perform effective condensation on partial-label datasets. In contrast, most existing dataset condensation methods rely on the assumption of having single labels for each instance and therefore fail under this type of supervision. The only exception lies in decoupled condensation approaches such as *RDED* and *SRE2L*, where a teacher model can still be trained on partial-label data. We present the corresponding results under partial-label supervision below in Table 9.

As shown in the table, our method consistently achieves substantial improvements across both Random and Class-50% candidate set generation strategies, and under all IPC settings. In particular, on Fashion-MNIST, our approach yields dramatic performance gains, reaching above **87%** accuracy even with partial label supervision, whereas both *RDED* and *SRe2L* fail to exceed 16% under the same setting. On the more challenging CIFAR-10 benchmark, our method also demonstrates strong robustness, especially under larger IPCs where the gap over baseline methods becomes increasingly pronounced (e.g., over **20%** absolute improvement at IPC = 100). These results highlight that our condensation strategy can effectively leverage weak supervision and generate compact yet highly informative synthetic datasets, even when label noise is introduced by the partial-label scenario.

Table 9: Classification results (test accuracy, %) on partial-label Fashion-MNIST and CIFAR-10 datasets under different IPCs. ‘Random’ and ‘Class-50%’ denote two candidate set generation strategies. **Bold** numbers indicate the best performance.

Dataset	Random				Class-50%			
	IPC	<i>RDED</i>	<i>SRe2L</i>	<i>Ours</i>	IPC	<i>RDED</i>	<i>SRe2L</i>	<i>Ours</i>
F-MNIST	1	10.48±0.82	9.72±1.02	<b>44.06±1.64</b>	1	10.73±0.78	10.93±0.76	<b>33.99±2.48</b>
	10	13.17±4.66	8.80±0.70	<b>72.02±0.77</b>	10	14.58±1.19	10.83±0.35	<b>70.46±0.26</b>
	50	13.06±2.36	10.30±0.40	<b>83.98±0.12</b>	50	15.55±0.55	11.33±0.76	<b>79.67±0.13</b>
	100	13.39±2.40	9.34±1.77	<b>87.30±0.31</b>	100	11.90±2.67	11.05±0.77	<b>81.42±0.25</b>
CIFAR-10	1	15.32±1.72	<b>20.69±0.88</b>	16.31±1.54	1	14.52±1.06	15.55±0.91	<b>16.61±1.14</b>
	10	26.28±0.29	19.45±1.12	<b>30.50±0.27</b>	10	10.00±0.00	18.56±0.05	<b>25.00±0.70</b>
	50	34.96±0.92	20.56±0.71	<b>44.39±0.65</b>	50	25.59±1.32	19.39±1.09	<b>45.94±1.27</b>
	100	28.88±2.56	19.65±1.09	<b>58.46±0.64</b>	100	25.81±1.64	18.65±1.51	<b>58.06±0.32</b>

## F RELATED WORK

### F.1 ROBUST DIFFUSION MODELS

Training robust conditional diffusion models under limited or imprecise supervision remains a relatively underexplored direction. Recent works have started to tackle this challenge by tailoring diffusion models to specific forms of weak or noisy information. For example, noise-robust diffusion models (Na et al., 2024; Li et al., 2024) focus on mitigating the effect of corrupted labels during training; positive-unlabeled diffusion models (Takahashi et al., 2025) leverage positive samples along with large amounts of unlabeled data to approximate conditional distributions; and semi-supervised diffusion (Givens et al., 2025; Ouyang et al., 2023) models aim to utilize both labeled and unlabeled data to improve conditional generation.

### F.2 IMPRECISE LABEL LEARNING

Imprecise label learning aims to address scenarios where the supervision signals are incomplete, ambiguous, or corrupted, thereby deviating from clean ground-truth labels. Existing studies can be broadly categorized according to the type of imprecision present in the dataset, including partial-label learning (Feng et al., 2020; Wu et al., 2022; Tian et al., 2023; Lv et al., 2020; Wang et al., 2025b; Xia et al., 2022; Wu et al., 2024), where each instance is associated with a candidate set of labels containing the true label; semi-supervised learning (Berthelot et al., 2019b; Zhang et al., 2021a; Yang et al., 2022; Wang et al., 2022c; Rasmus et al., 2015; Zheng et al., 2022), where only a small subset of samples are labeled while the majority remain unlabeled; and noisy-label learning (Han et al., 2018; Wei et al., 2021; Han et al., 2020; Goldberger & Ben-Reuven, 2017; Liu et al., 2020), where the observed labels are corrupted versions of the true labels. Beyond these canonical settings, there is also growing interest in mixture imprecise-label learning (Chen et al., 2024a; Zhang et al., 2020; Wei et al., 2023; Shukla et al., 2023; Xie et al., 2024), which combines multiple forms of imprecision within a unified framework to better reflect the complexity of real-world data.

### F.3 DATASET CONDENSATION

Dataset distillation (DD) (Wang et al., 2018) compresses a large labeled dataset into a compact synthetic set that preserves task-relevant information, thereby reducing training cost while retaining accuracy comparable to training on the full dataset. Approaches include *bi-level optimization*, which learns synthetic data whose training signals emulate those of the original data via *gradient*

*matching* (Zhao et al., 2021; Lee et al., 2022; Kim et al., 2022), *trajectory matching* (Cazenavette et al., 2022a; Cui et al., 2023; Guo et al., 2024), and *meta-model matching* (Wang et al., 2018; Nguyen et al., 2021; Loo et al., 2022; Zhou et al., 2022; He et al., 2024); these methods often achieve high fidelity but incur notable computational and memory costs. A second stream, *distribution matching*, aligns pixel-, feature-, or kernel-space statistics between synthetic and original data to improve efficiency (Wang et al., 2022b; Liu et al., 2022; Sajedi et al., 2023; Shin et al., 2024; Xue et al., 2025). Complementing these, *decoupled optimization* increases efficiency by removing the inner–outer dependency of the bi-level framework, for example, by matching running statistics embedded in a pretrained model or by leveraging pretrained models to select class-preserving crops from the original dataset. Representative methods (Yin et al., 2024; Sun et al., 2024) have scaled DD to large-scale settings and motivated follow-ups that broaden feature-statistic alignment and stabilize optimization protocols (Shao et al., 2024; Yin & Shen, 2024).

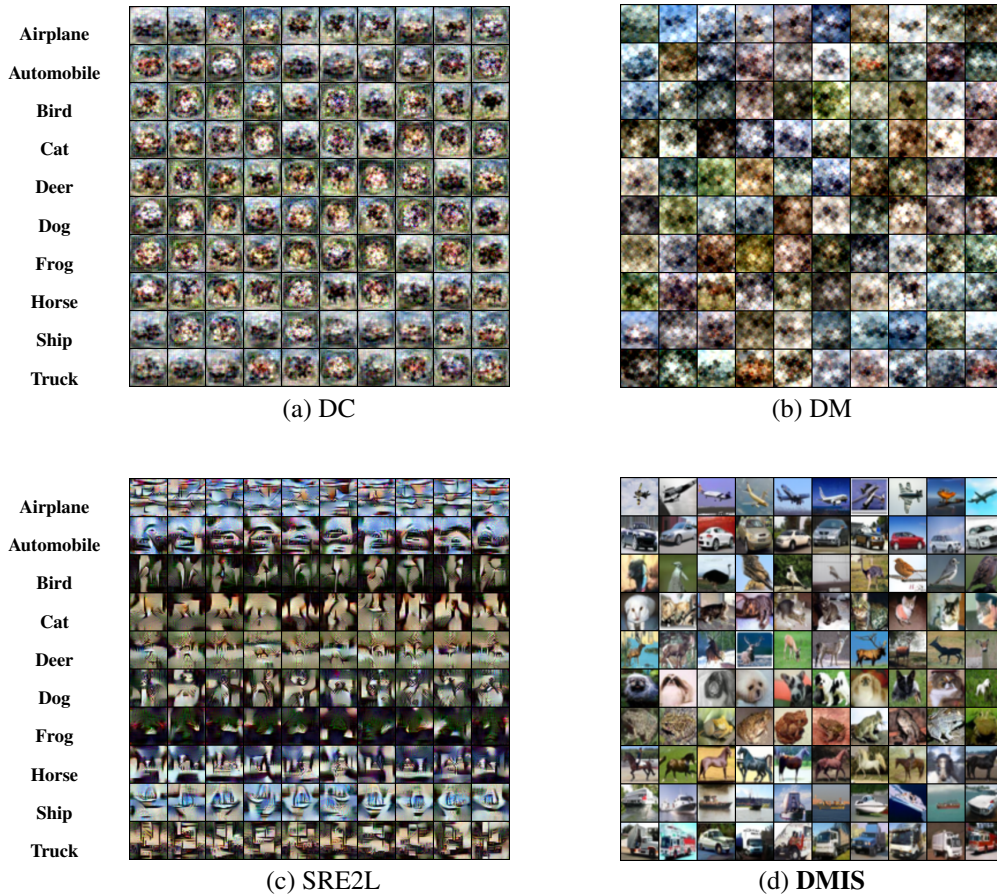


Figure 8: Visualization of condensed CIFAR-10 images generated by *DC*, *DM*, *SRE2L*, and our method *DMIS*.

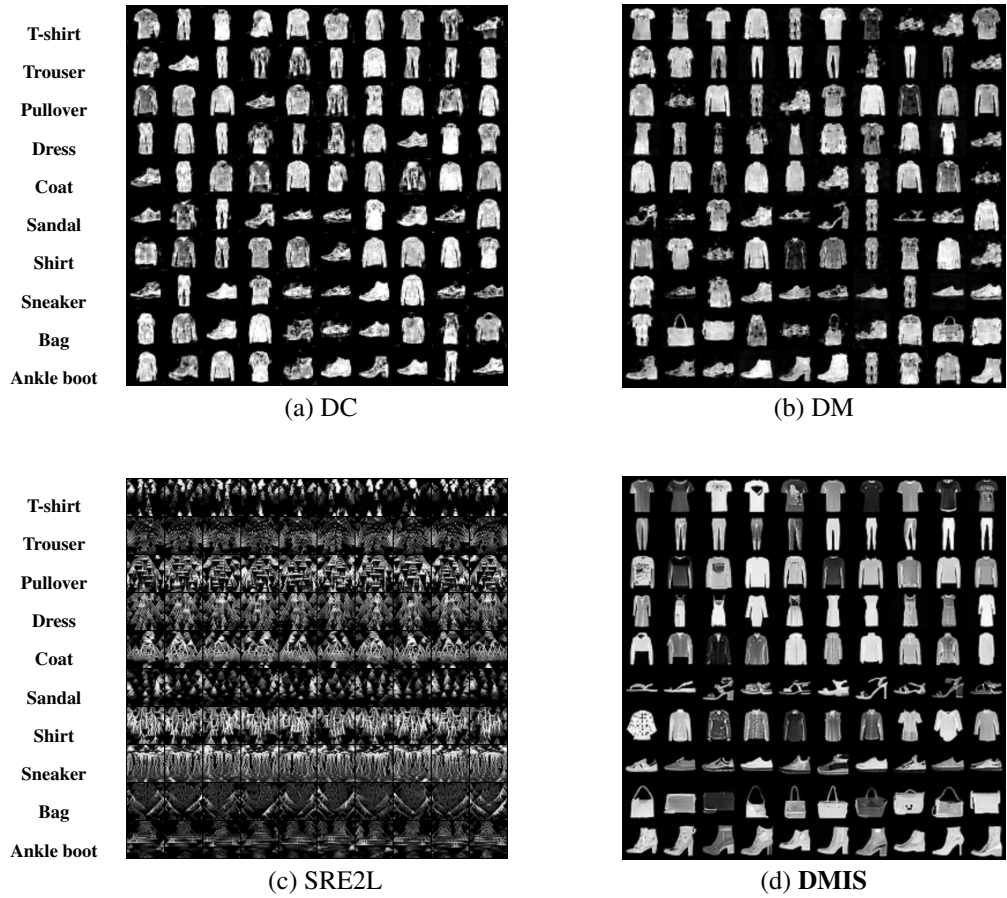


Figure 9: Visualization of condensed Fashion-MNIST images generated by *DC*, *DM*, *SRE2L*, and our method *DMIS*.